Experimental and numerical investigations on slender panels with holes under symmetrical localised loads

# Experimental and numerical investigations on slender panels with holes under symmetrical localised loads

Maiorana E*[a], Tetougueni CD[b], Zampieri P[b], Pellegrino P[b]

[a]*Isolcomit Srl, Via Roma 7, 35020 Legnaro, Italy*

[b]*Department of Civil, Environmental and Architectural Engineering, University of Padova, Via Marzolo 9, 35131 Padova, Italy.*

* Corresponding author:

**Abstract:**

Perforated steel girders under a single or combined in plane loading has been largely studied in the literature. However, such investigations were trusted on the numerical modelling and FEM analysis and due to the lack of experimental results in most cases, the accuracy of the numerical model and the consideration of imperfections in the FEM analyses are open to reflexion. In this paper, a series of experimental tests are performed to study the post-critical behaviour of perforated steel girders. Ten full scales steel girders were tested under uniaxial compressive force. Amongst them, four were used as control specimens whereas a circular hole was located in the center of the other six. The parameters such as the geometry of the web plate, the position of the hole and the plate slenderness are found as those most influencing the post-critical behaviour. Finally, the experimental results were used to validate the intensive numerical analyses. The results obtained showed the strong influence of combined geometrical imperfections and residual stresses on the mid-plane Von Mises stresses.

*Keywords: perforated steel plate, buckling, post-critical load, steel bridges girder*

**List of Notations**

| | |
|---|---|
| $\nu$ | Poisson's ratio |
| $h_w$ | Web height |
| $t_w$ | Web thickness |
| $\lambda_w$ | Plate slenderness |
| $t_f$ | Flange thickness |
| $b_f$ | Flange width |
| $s_s$ | Patch loading length |
| $f_{yd}$ | Yielding design strength |
| $f_{ud}$ | Ultimate design strength |
| $a$ | Width of the panel |
| $F_{sd}$ | Design external load |
| $F_{Rd}$ | Design resistance |
| $F_R^y$ | Web yield strength |
| $F_R^b$ | Load limit corresponding to the global instability |
| $F_R^c$ | Critical buckling load of the web section |
| $E_s$ | Young Modulus |
| $f_{wd}$ | Web design strength |
| $k$ | Buckling coefficient |
| $L_{eff}$ | Effective resistant length |
| $t_{st}$ | Thickness of the vertical stiffener |
| $b_{st}$ | Width of the vertical stiffener |
| $F_{u,n°;\Delta mm}$ | Ultimate strength of the imperfect girder |
| $n°$ | Initial modal shape |
| $\Delta mm$ | Amplitude of the modal shape |
| $F_{cr}$ | Critical buckling load |
| $F_{u,exp}$ | Experimental ultimate strength |

## 1. Introduction

In the past years many bridges have been constructed using the incremental launching process since the technique presents several advantages in time and material consuming. Besides, this methodology is particular effective to overcome, for example, deep valleys, environmentally protected species and deep-water crossings. It implies that part or all the bridge superstructures are assembled in factories and then when in-situ, they are pulled longitudinally from one side to its final position. The method is convenient for bridges where girders are made of steel material to take advantages of the lightness of the material. However, due to the bearing located at each bridge pier, a compression force as the result of the superstructure self-weight is prone to arise during the process. The situation may cause a reduction of the ultimate capacity of the girder if adequate measures are not taken to limit the risk. This observed decrease in strength and critical load is valid for both perforated and non-perforated steel sheets. For this reason, vertical stiffeners are provided to avoid at maximum this effect. Several authors have shown their interest in this topic [1-6] since many articles addressing both stiffened and unstiffened plate stability are still published nowadays.

From previous studies, thin steel holed plates are widely used in many engineering fields. For instance, ship structures, bridge engineering, offshore as well as aerospace structures are made of steel plate [7]. From various reasons, the presence of openings is often indispensable. In particular, the maintenance and inspection routine are one of the major reasons of the presence of holes in girders [8]. The structural behaviour of a perforated plate may be affected due to a redistribution of normal and shear stresses leading to a considerable reduction of ultimate strength and critical buckling of steel plates [8-9]. For this reason, a large amount of research [10-12] has been carried out in order to better understand the modification in the failure mechanism of steel plate due to holes' presence.

In particular, many authors made their studies on elastic stability under axial compression [13-17]. Maiorana et al. [13], performed throughout Strand7 [18] analyses on steel plates under symmetrical localized load, with circular and rectangular holes. The authors considered a patch loading applied on several simply supported rectangular plates. Different behaviours were observed accordingly to the stress level. For example, non-linear analyses of the plate reveals plasticization of the area near the hole, causing the two parts of the plate separated by the hole to slip. On the other hand, collapse generally happens on slender rectangular panels due to buckling before yielding with the formation of two shear strips on the web plate [13]. Cheng et al. [14], were able to demonstrate the influence of parameters such as slenderness ratio, hole width, plate width, hole aspect ratio on ultimate strength and stress concentration on steel plates with a slotted hole subjected to uniform displacement. Investigations conducted showed that the perforated specimens collapsed under the combined effect of global and local buckling. Moreover, the authors found that the panel aspect ratio not exceeding 2.0 likely influences the stress concentration factors of the plate. Others have found that the maximum stress concentration occurs at the perimeter of the cut [19] and that the aspect ratio of the plate influences the ultimate strength of the perforated plates while the normalized ultimate shear strength is not entirely influenced by the thickness of the plate [20]. El-Sawy and Nazmi [9] studied the effect of the hole location, panel aspect ratio,

and plate geometry on the buckling coefficient of perforated rectangular plates subjected to uniaxial compression. The results showed that girders with rectangular hole are more rigid than plates with circular hole. Besides, an optimal range of the hole geometry interval for the use of a circular hole was derived. Finally, the authors gave recommendations on hole diameter to avoid a decrease in the critical buckling load of the plates.

Recently, many research activities have been done to deepen the behaviour of perforated panels [21-24]. Specifically, the effects of holes on the behaviour of the sheets has been studied in [25-26]. For circular holes, in [11-12], for rectangular shapes in [27-30] under various loading conditions. Komur and Sonmez [31], analysed the perforated plates subjected to in-plane compressive edge loading. The authors considered four different edge loading cases and discussed the influence of the load location to the buckling load. They found that the concentrated edge load to the plate leads to a consistent reduction of the buckling coefficient of square panel. Furthermore, their study showed that the size of hole doesn't directly influence the buckling load parameter for rectangular plate. El-Sawy and Nazmi [9] found the increase of the hole's size led to a decrease of the critical stress in the case of thick panel. However, the failure is not due to the plate instability by to the attainment of the ultimate resistance. In addition, the grade of the steel used will strongly impact the critical loads based on its yielding strength. El-Sawy et al. [32] found that the influence of the panel aspect ratio for a particular case of centered hole is limited. Another studies on the optimal location that may follow circular and rectangular in the case of combined bending moment and axial force are found in [9], [33]. Sharkerley and Brown [33] defined mechanisms to explain the behaviour of steel plates with perforations of various sections and found a good agreement with other results. Sharkeley and Brown [33] presented the parameter, which has a major effect on the critical buckling load. For square plates with rectangular perforations, the ultimate load will be reduced according to the elastic instability that occurs prior to the plate yielding. Furthermore, they found that the perforation major dimension should not be perpendicular to the load axis.

The post-critical buckling mechanisms in the case of high-grade steels is limited when the perforated plate is subjected to localized symmetrical loads. Indeed, for cost limitation, a slender plate is considered for high-grade steel. Extensive finite element analysis using Abaqus aimed to study the behaviour on post-buckling of a perforated plate as in Shanmugam et al. [34] have been performed to study its ultimate load capacity under axial compression. The slenderness ratio and hole's size, as well as the external condition of the edge, are considered as affecting the ultimate load of the perforated plate.

According to the literature, the need to improve the knowledge of the post-critical behaviour of perforated steel plates through an innovative approach is clearly described and justified by the lack of experimental tests on full-scale steel beams. Indeed, many research activities on the argument in the past were based on intensive FEM analysis attempting to define accurate numerical models. In this study, the authors provided a solid background for future investigations, as they conducted extensive experimental tests to evaluate the critical behaviour of perforated beams. The geometries of the rectangular and square panels with a centred and eccentric hole have been studied. At the same time, the study of the out-of-plane behaviour of the I-section steel element was made possible by a non-linear finite element analysis taking into account the

behaviour of the elastoplastic material, initial geometric imperfections and residual stresses. Finally, a further evaluation was carried out to determine the influence of the percentage load applied on the von mises stress state and ultimate strength. Based on the numerical results, the authors stressed the need to develop new design equations in the standards since the existing equations still provide conservative results for the strength of steel plates with and without holes.

## 2. Objectives

The main scope of this research is to investigate throughout extensive experimental campaign and FEM modelling the structural behaviour of perforated steel girders with various geometry and location of the hole. The first part of the work, consisted in investigating recent studies on steel plate's stability with and without openings, the results of which were discussed in the introduction, and then the experimental programme will be presented before the FEM analysis. Specifically, to reach our goals, the sub-objectives of the study were defined as follow:

- To observe the structural behaviour of rectangular and squared girders with two different slenderness values in the elastic and plastic range;
- To examine both the load carrying capacities and the failure modes of perforated sections.
- To examine the positions of high stress concentration points in the vicinity of the application load region.
- To accurately calibrate the numerical model on the base of the experimental campaign and integrating imperfections and residual stresses.
- To correlate the experimental results with FE models, and thoroughly investigate their complex structural behaviour in terms of post-buckling load, stress distribution and failure mode.

The document will be presented in five parts. After the introduction and the objectives of the research, the experimental campaign will be described, starting with a brief theoretical background, followed by the test set-up, sample details, material characteristics, test procedure before the introduction of the FEM analysis. The last point before the conclusion will be the presentation and discussion of the experimental and FEM results.

## 3. Experimental programme

### *3.1. Introduction*

In civil engineering, the empirical approach is quite important even though it requires more costs and controls since it helps to validate and extend the theoretical background, provides qualitative and quantitative indication for FEM analysis. In this study. An experimental campaign was conducted on ten full scale S355J0

steel perforated specimens in the laboratory of University of Padova Department ICEA. Afterwards. the adopted constraints condition in the tests and results found were used to investigate more in depth the post-critical failure of the perforated girders throughout parametric analyses.

### *3.2. Steel girder under localized loads*

The classification of the buckling behaviour of steel plates according to their slenderness has been discussed in [35]. In general, the stress versus lateral deflection curve for both stocky and slender steel girders under compression load is shown in Fig. 1. In particular, in the case of slender plates (Fig. 1a), the geometrical bifurcation will be observed after a large out of plane displacement. It is a common situation at $\sigma_{fail}$ and web breathing may rise limiting the use of the available extra-strength in the post-buckling domain. Stocky plates on the other hand will show plastic buckling after elastic limit of the material (Fig. 1b) and the ultimate stress is in this case similar to the stress at failure. The material bifurcation takes place after the post-yield capacity is reached [35].

The design of the steel plate under a localized loading condition is usually done in accordance with the existing standards. The design formulas were developed in base of the theoretical background or intensive experimental campaigns. In this section, the theoretical background of the steel plate subjected to vertical loadings is presented. From the Italian guideline CNR 10011/97 [36], the following checks should be integrated.

$$F \leq \frac{230000}{\nu} \cdot t_w \cdot b_f \cdot [1 + 2 \cdot (\frac{h_w}{a})^2] \cdot (\frac{t_w}{h_w})^2 \quad (1)$$

$$F \leq 1{,}15 \cdot t_w \cdot (s_s + 2 \cdot t_f) \cdot f_{yd} \quad (2)$$

Where $\nu$, $h_w$, $t_w$, $t_f$, $b_f$, $s_s$, $f_{yd}$ and a, represent respectively the poisson's ratio, the web height, the web thickness, the flange thickness, the flange width, the patch loading length, the design yielding strength of the plate and the width of the panel.

The integration of the previous instructions for stiffened web panel as described in CNR 10030/87 [37] requires the following general equations to be verified under localised loads:

$$F_{sd} \leq F_{Rd} \quad (3)$$

With:

$F_{sd}$ and $F_{Rd}$ respectively the design external load and the design resistance.

$$F_{Rd} = \min(F_R^y, F_R^b, F_R^c) \quad (4)$$

$$F_R^y = (s_s + 2 \cdot \beta \cdot t_f) \cdot t_w \cdot f_{wd} \quad (5)$$

$$F_R^b = \sqrt{2 \cdot \beta \cdot E_s \cdot f_{wd}} \cdot \left(\frac{b_f}{10 \cdot t_f}\right)^{1/4} \cdot \sqrt{k \cdot \frac{t_w}{h_w} \cdot t_f \cdot t_w^3} \quad (6)$$

$$F_R^c = \sqrt{E_s \cdot f_{wd} \cdot \frac{t_f}{t_w}} \cdot 0{,}45 \cdot t_w^2 \cdot \left[1 + \frac{3 \cdot s_s}{h_w} \cdot \left(\frac{t_w}{t_f}\right)^{3/2}\right] \quad (7)$$

Where $F_R^y$ is the web yield strength under the localized load, $F_R^b$ is the load limit corresponding to the global instability and $F_R^k$ the critical buckling load of the web section.

With $E_s$, $f_{wd}$, $s_s$, $\beta$ are the young modulus, the web design strength, the length of the loaded part and $k$ the coefficient defined in Eq. (8-9).

$$k = 2 + 4 \cdot \left(\frac{h_w}{a}\right)^2 \text{ for hinged web} \quad (8)$$

$$k = 5.5 + 4 \cdot \left(\frac{h_w}{a}\right)^2 \text{ for fixed web} \quad (9)$$

Finally, the European standard EC 3-1-5 [38] aims at verifying the strength of the cross-section of the panel with a single formula; for cross-sectional actions the verification criterion is as follows:

$$F \leq f_{yd} \cdot t_w \cdot L_{eff} \quad (10)$$

Where $L_{eff}$ is the effective resistant length. Additional information can be found in standards [38]. Finally, it should be stressed that this verification procedure applies to both rolled and welded beams, as the loading length $s_s$ is less than the width of the web panel [38]. The comparison was therefore made possible since the dimensions of the experimental specimens are within the range of validity of the verification of the standards.

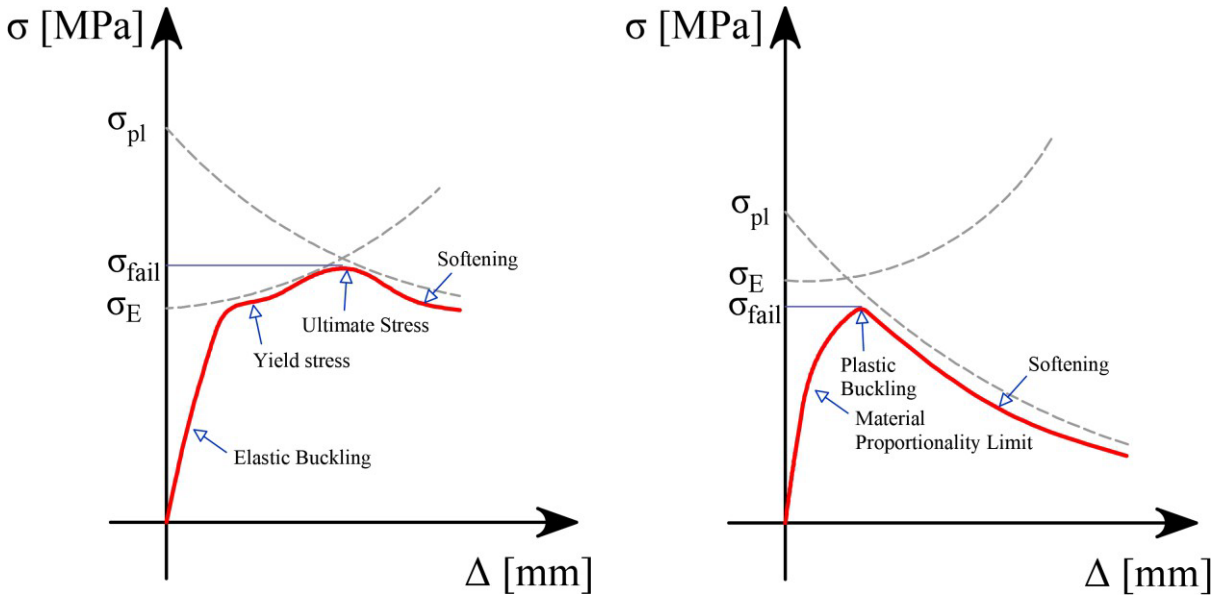


a) Slender plate b) Stocky plate

Fig. 1: Stress versus lateral deflection in steel plates

*3.3. Test setup*

For the execution of the experimental tests, the equipment supplied by the laboratory of the University of Padova was used. The load application on the test samples was possible through a hydraulic jack supported by a steel portal. Both components were chosen to have a possible applied load higher than that of the ultimate load of the web panels. The apparatus for the testing programme was arranged in such a way that the speed of the hydraulic jack was under control to manage different rate of energy applied to the samples. Fig. 2 shows the experimental setup.

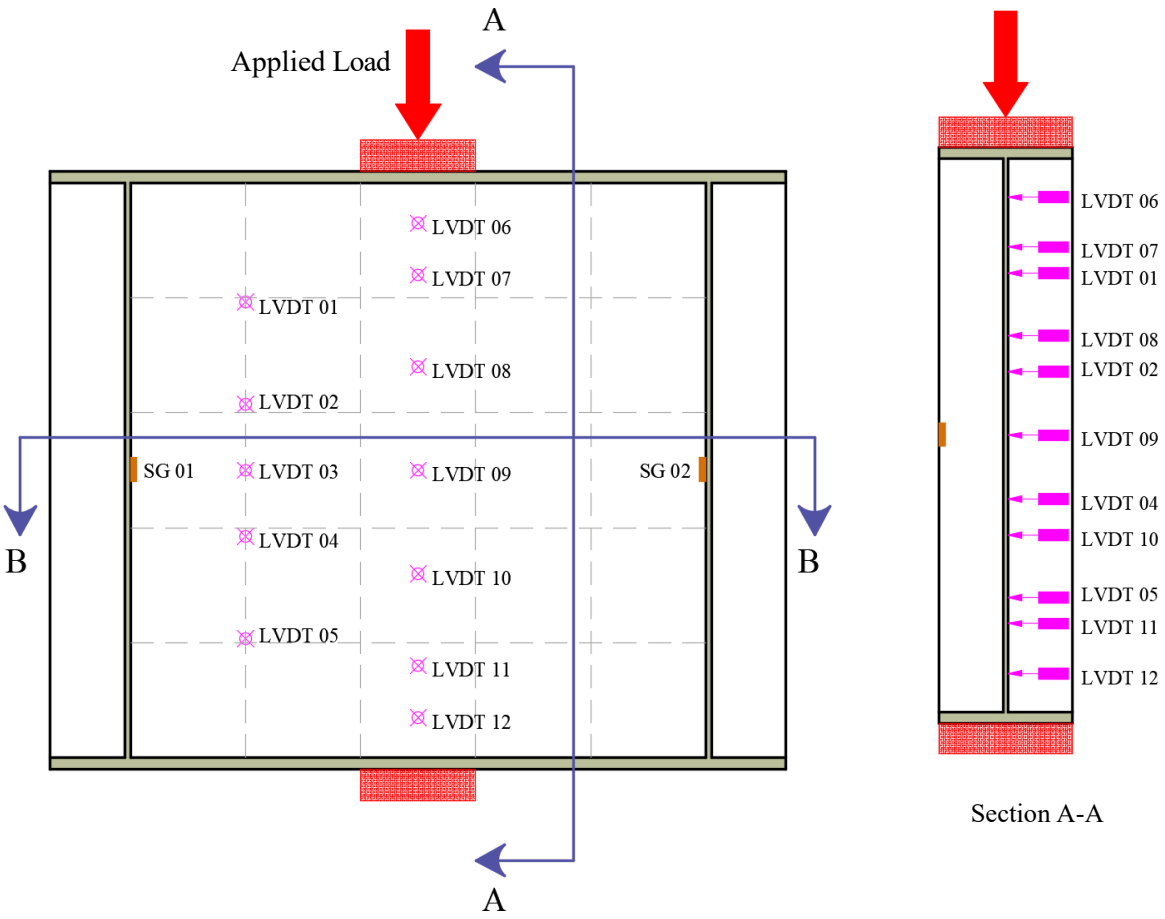

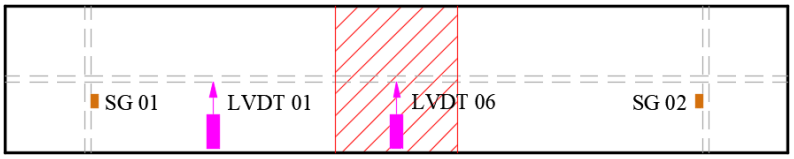


Section B-B

a) square girder setup

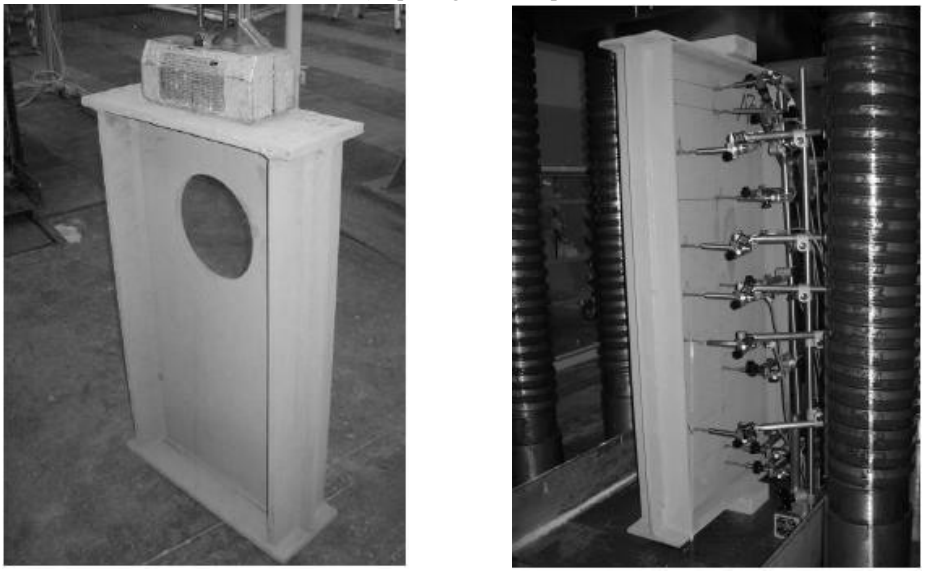

b) rectangular girder setup

Fig. 2: Test setup and Laboratory apparatus for the experimental tests

### *3.4. Details of specimens*

The choice of the specimens should reflect as maximum as possible the current practices in the bridge industry. In this regards, two different girder's geometries have been considered. The depth of the web openings was limited at maximum to $0.5 \cdot a$ as suggested in [39] to prevent Vierendeel effects before the post critical buckling failure of the web. Two series of web panels (A and B) characterized by different values of slenderness $\lambda_w$ were considered. For each control panel, a companion panel with the presence of hole were associated. In total, ten specimens were tested with an identical loading condition for each test. In Fig. 3, all the information related to the five samples A is presented. It is should be highlighted that the samples B differ only to the sample A by their slenderness ratio and have not been presented in Fig. 3. Finally, Table 1 summarizes the geometrical and loading characteristics of the samples.

Table 1: Geometrical characteristics and details of the specimens in the experimental campaign

| Sample nomenclature | $h_w$ (mm) | $a$ (mm) | $t_w$ (mm) | $\lambda_w$ (mm) | $b_f$ (mm) | $t_f$ (mm) | $b_{st}$ (mm) | $t_{st}$ (mm) | $d/a$ | $c/h_w$ | $s_s/a$ |
|---|---|---|---|---|---|---|---|---|---|---|---|
| 1A | 500 | 500 | 5 | 100 | 120 | 10 | 50 | 5 | - | - | 0.2 |
| 2A | 500 | 500 | 5 | 100 | 120 | 10 | 50 | 5 | 0.5 | 0.5 | 0.2 |
| 3A | 1000 | 500 | 10 | 100 | 140 | 10 | 60 | 1 | - | - | 0.2 |
| 4A | 1000 | 500 | 10 | 100 | 140 | 10 | 60 | 10 | 0.5 | 0.515 | 0.2 |
| 5A | 1000 | 500 | 10 | 100 | 140 | 10 | 60 | 10 | 0.5 | 0.24 | 0.2 |
| 1B | 500 | 500 | 10 | 50 | 120 | 10 | 50 | 10 | - | - | 0.2 |
| 2B | 500 | 500 | 10 | 50 | 120 | 10 | 50 | 10 | 0.5 | 0.5 | 0.2 |
| 3B | 1000 | 500 | 20 | 50 | 220 | 20 | 90 | 20 | - | - | 0.2 |
| 4B | 1000 | 500 | 20 | 50 | 220 | 20 | 90 | 20 | 0.5 | 0.505 | 0..2 |
| 5B | 1000 | 500 | 20 | 50 | 220 | 20 | 90 | 20 | 0.5 | 0.24 | 0.2 |

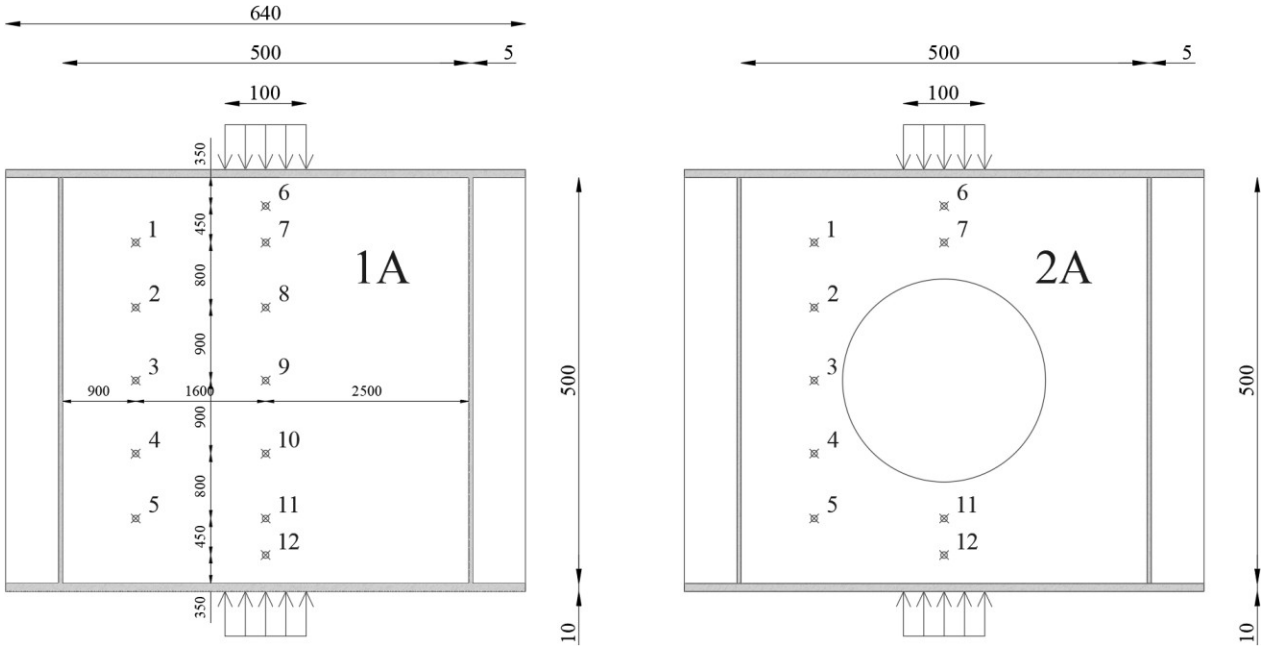


a) square web panels

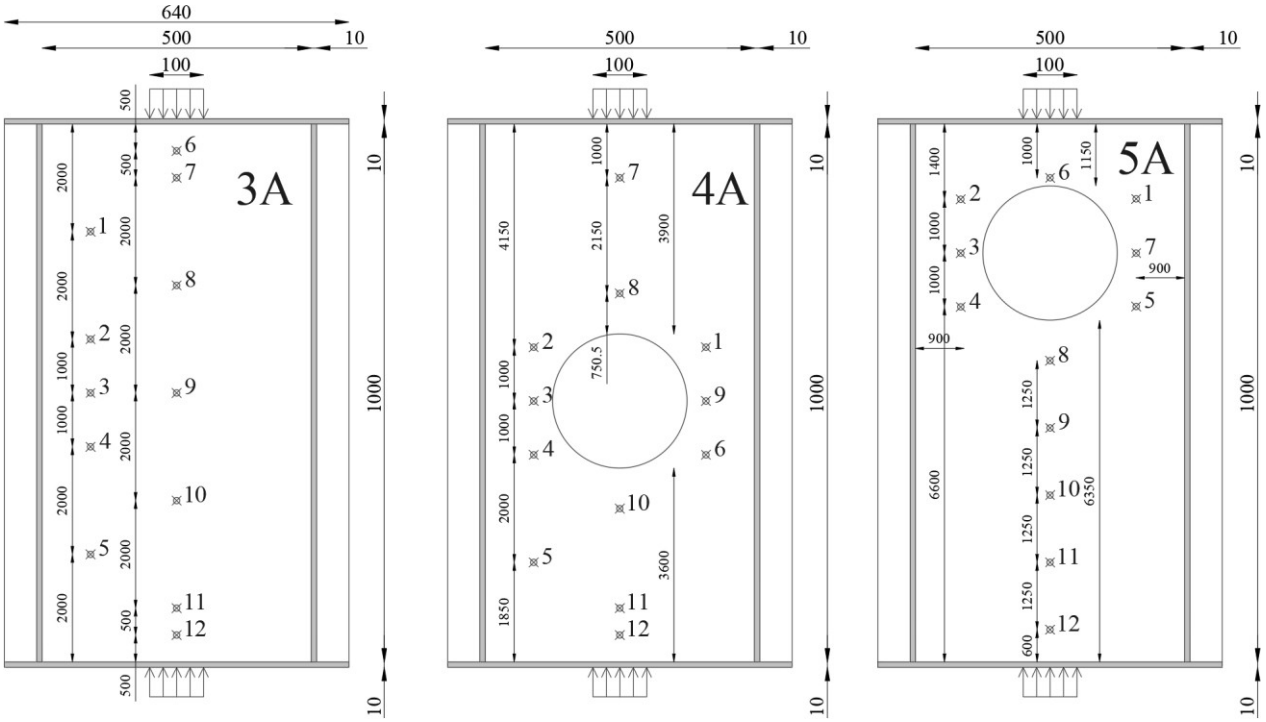


b) rectangular web panels

Fig. 3: Characteristics and position of the extensometers in the experimental tests

### *3.5. Test procedure*

The steel girders were subjected to uniaxial load through a displacement control protocol. The specimens were tested in a test machine with a capacity of 10 MN, on which a force transducer with a capacity of 6 MN was mounted, in a displacement control mode at 0.5 mm/min. The patch loading was transmitted to the upper flange of each sample by means of a non-deformable steel loading plate (Fig. 2b. It should be noted that a 50 mm thicker beam was used to transfer the load to the girder tested while its width of 100 mm was chosen to match the patch loading length. On the opposite side of the panel, the stress is balanced by a support located at the lower flange with the length equal to that of the applied patch loading. The resulting static scheme is as follows (see Fig. 4a):

a) experimental test layout b) measurement sections

Fig. 4: Details in the experimental test and survey activity

Axial strains were monitored though a couple of stain gauges (SG01 and SG02) located on vertical stiffeners. For the measurement of displacements under load, several linear voltage displacement transducers (LVDTs) were used. These instruments were placed in contact with the web panel as shown in Fig. 2 in some significant points and starting from the initial configuration, they directly detect the displacements that the steel plate displays. In addition, they are used to record the out-of-plane displacement of the panel as the load increases. During the test, they were placed along the height of the web girder to reconstruct the deformation trend for the entire height of the panel. All the measuring instruments were connected to the "Spider" acquisition devices, which had the task of transferring the collected data to a computer, which in real time collects and stores the results and organizes them in a spreadsheet.

### *3.6. Material characterization*

Before the study of the post-critical buckling of the girders, the mechanical property of the material was experimental evaluated, which is an important step for the numerical modelling as well. Five dog-bones tensile test samples cut from the built-up steel beam specimen were prepared and tested according to [40]. The average measured tensile properties is summarized in Table 2.

Table 2: Average mechanical tensile properties of steel.

| Samples | 1 | 2 | 3 | 4 | 5 |
|---|---|---|---|---|---|
| section ($mm^2$) | 10 x 29.3 | 9.9 x 29.5 | 10 x 30.3 | 9.9 x 30 | 10 x 29.6 |
| $d_{eq}$ (mm) | 19.31 | 19.28 | 19.64 | 19.45 | 19.41 |
| $f_{yd}$ (MPa) | 343 | 344 | 353 | 340 | 347 |
| $f_y$ (MPa) | 360 | 361 | 371 | 357 | 364 |
| $f_u$ (MPa) | 520 | 525 | 521 | 524 | 525 |
| $A_5$ (%) | 34.7 | 34.2 | 33.1 | 36 | 38.7 |

Where $A_5$ represents the elongation ratio at failure with the reference length equal to five times the equivalent diameter of the dog-bone.

### *3.7. Experimental results*

From the experimental campaign, the ultimate resistance of the ten samples (intact and perforated girders) were collected and summarized in Fig. 5. The results show that the decrease of slenderness may increase the capacity of a normal girder from 1.9 to 4.4 times dependently of its geometry while the presence of a hole in the web leads to a reduction of the strength. Indeed, for slender panel, the ultimate load may be

reduced up to 24% accordingly to the geometry of the plate and the position of the holes, whereas for thick panel the loss of the capacity can reach 29 % of the ideal plate (see Table 3). On the other hand, the European standard [41] provides always higher ultimate loads than those obtained through Italian standards [36, 37], especially in the case of the thick girders (samples B). Finally, in most cases, CNR 10030 [37] standard provides higher ultimate resistance values compared to those proposed by CNR 10011 [36]**.** Both have proven, however, to be largely conservative while in the case of the perforated panel, they are no longer reliable.

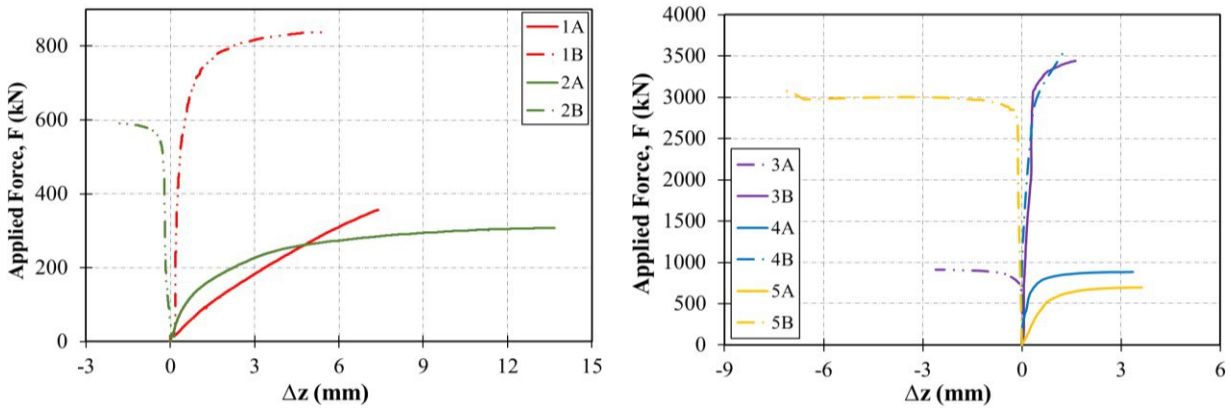


a) square girder b) rectangular girder

Fig. 5: Ultimate resistance of girders under compression loads

Table 3: Ultimate capacity of steel girders under compressive loads

| Sample nomenclature | $F_{u.exp}$ (kN) | $F_{u.CNR10011}$ (kN) | $F_{u.CNR10011}$ / $F_{u.exp}$ | $F_{u.CNR10030}$ (kN) | $F_{u.CNR10030}$ / $F_{u.exp}$ | $F_{u.EC3}$ (kN) | $F_{u.EC3}$ / $F_{u.exp}$ |
|---|---|---|---|---|---|---|---|
| 1A | 357.3 | 172.5 | 48.3% | 162.7 | 45.5% | 174.8 | 48.9% |
| 2A | 307.8 | 172.5 | 56.0% | 162.7 | 52.9% | 174.8 | 56.8% |
| 3A | 911.9 | 476.8 | 52.3% | 493.5 | 54.1% | 673.1 | 73.8% |
| 4A | 883.5 | 476.8 | 54.0% | 493.5 | 55.9% | 673.1 | 76.2% |
| 5A | 695.9 | 476.8 | 68.5% | 493.5 | 70.9% | 673.1 | 96.7% |
| 1B | 837.1 | 556.3 | 66.5% | 650.8 | 77.7% | 790.3 | 94.4% |
| 2B | 591.4 | 556.3 | 94.1% | 650.8 | 110.0% | 790.3 | 133.6% |
| 3B | 3442.7 | 1112.5 | 32.3% | 1382 | 40.1% | 3126.2 | 90.8% |
| 4B | 3578 | 1112.5 | 31.1% | 1382 | 38.6% | 3126.2 | 87.4% |
| 5B | 3089.1 | 1112.5 | 36.0% | 1382 | 44.7% | 3126.2 | 101.2% |

## 4. FEM analysis

### *4.1. Introduction*

Global finite element analyses on full-scale perforated panels were carried out after the experimental campaign. The first numerical model was calibrated based on test results and then a series of nonlinear parametric analyses was performed on the replicated beam samples to extend the considerations to other cases and configurations. In addition to the non-linear analyses, the comparisons will be integrated with the results

deduced from the solution of the linear buckling problem; these are carried out on the panel considered perfectly flat. From the comparisons between the critical load value, the maximum experimental resistance and the one resulting from the non-linear analysis, it will be possible to make the necessary observations as the shapes and dimensions of the panels vary.

### *4.2. Model Description*

The numerical analysis has been done throughout Strand7 [18]. The mesh was done with (Quad4) plate elements of typical size equal to $a/20$ (see Fig. 4a) and each node has six degrees of freedom. However, in the case of perforated web panels, the shape and size of the mesh surrounding the hole were variable and such as to adapt to the rest of the mesh. Vertical loads were applied directly to the flanges as a system of conservative force. Out-of-plane displacement was prevented with a proper constraint along the connection points between the web and flanges while the transversal constraints were applied at the two projected center node to the flanges.

The material properties from a S355 steel grade were similar for the web, flanges and stiffeners. The Newton-Raphson solution approach was used in the analysis to consider the material and geometry nonlinearity. The Young modulus adopted and the Poisson coefficient were respectively 206,000 MPa and 0.3. From the tensile tests conducted on five specimens of the same material constituting the panels, it was possible to obtain a simplified average value curve σ-ε. Then, trilinear curves with plateau were adopted and characteristics are summarized in Table 4.

Table 4: Material characteristics in FEM analysis

| Branch | 1st branch | 2nd branch | 3rd branch |
|---|---|---|---|
| σ (MPa) | 0 – 345.4 | 345.4 - 498 | 498 |
| E (MPa) | 206,000 | 4,300 | 0 |

To model the initial geometric imperfections, it was considered appropriate to consider among the possible solutions those deduced from a linear buckling analysis. It is important to add that the forms of imperfections taken into consideration were the first buckling shapes with the amplitude equal to min($h_w$/100; 5 mm) as referenced in [41] in the case of controlled welding process. The sensitivity analysis of the geometrical imperfections was studied considering various magnitudes between 0.75 mm to 5 mm. On the other hand, for profiles with welded section it is appropriate to consider, in addition to the geometrical imperfections, the state of self-tensioning generated by welding operations. Several authors presented in their research the necessity to take into account the amplitude and shape of the residual stress in the FEA [42-43]. In the present study, with the absence of the experimental measurements, the residual stresses were studied through a parametric process in such way to define the effective numerical model for each specimen. Indeed, for each numerical model, the behaviour of the sample under different ranges of residual stress will be studied; these will be characterized as a function of the percentage of the tensile stress peak. In particular, four different

situations were taken into consideration at each sample investigated, distinguished by the magnitude of the peak tensile stress $\sigma_{max}^{+}$ equal to 0, 70, 85 and 100% of the yield strength, i.e. about 0, 242, 293 and 345 MPa.

### *4.3. Model Verification*

The results from a sensitivity analysis are briefly presented to validate the choice adopted for the FE model investigated. Assuming a geometrically imperfect girder, the structural response was evaluated in the presence of self-tensioning field. As indicated in the previous subsection, various amplitudes of imperfections and residual stress were considered when calibrating the numerical modelling of each sample tested in the laboratory.

## 5. Experimental and FEM results

In this section, the out-of-plane displacement of the girder under compressive loads is analysed and discussed. Both experimental and numerical results will be displayed in the same graphs for a better comparison and each test specimen will be commented. In addition, the influence of the magnitude of the residual stress applied to the girders before the FEM analysis is discussed. Finally, two sections namely "middle" and "edge" (see Fig. 4b) are distinguished. It is important to highlight that for each sample, the influence of the geometrical imperfections and the residual stresses is studied. The results for selecting the most appropriate imperfections are first presented in tables using the term $F_{u,n^o;\Delta mm}$ indicating the ultimate strength of imperfect girder and then discussed, after which the influence of the residual stress will be evaluated.

### *5.1. Sample 1A*

Non-linear analyses have been performed to the girder where a half-wave deformed shape equivalent to the experimental observation was applied to the web. From the results, the slender girder showed a post-critical resistance reserve that increases the ultimate resistance by about 19% as shown in Table 5. Furthermore, the analysis revealed that the girder is quite influenced by the amplitude of the imperfection. In the rest of the study, it will be considered $\Delta$=0.75 mm of the imperfection since it expresses a closer result to the experimental observation. Indeed, the structural response of the girder was then studied with the presence of the residual stress. Four situations were investigated with, at each case, different value of the peak tensile stress $\sigma_{max}^{+}$. Fig. 6 illustrates the progression of out-of-plane displacements for some load levels for the four different FEM mesh with different maximum residual stresses in percentage. In all cases the initial deformation corresponds to the first buckling mode with a maximum amplitude of 0.75 mm. Experimental results (first series) have also been reported to obtain an immediate graphical comparison.

Table 5: Critical and ultimate load from FEM analysis

| $F_{u,exp}$ | $F_{cr}$ | $F_{u,1°;5mm}$ | $F_{u,1°;2.5mm}$ | $F_{u,1°;1.25mm}$ | $F_{u,1°;1mm}$ | $F_{u,1°;0.75mm}$ |
|---|---|---|---|---|---|---|
| 357.33 | 290.1 | 331.6 | 339.6 | 344.2 | 346.1 | 346.9 |
| - | 81.2% | 92.8% | 95% | 96.3% | 96.9% | 97.1% |

From Fig. 6, it can be seen that the effect of the residual stresses is considerable, even at early stage of load magnitude. The deformed shape remains almost unchanged, but the out-of-plane displacement measured grows significantly. From both graphs it can be seen that by including the residual stresses in the modelling, the numerical results are close to the experimental ones; this is particularly evident in the edge section up to loads equal to 95% of $F_{u,exp}$.

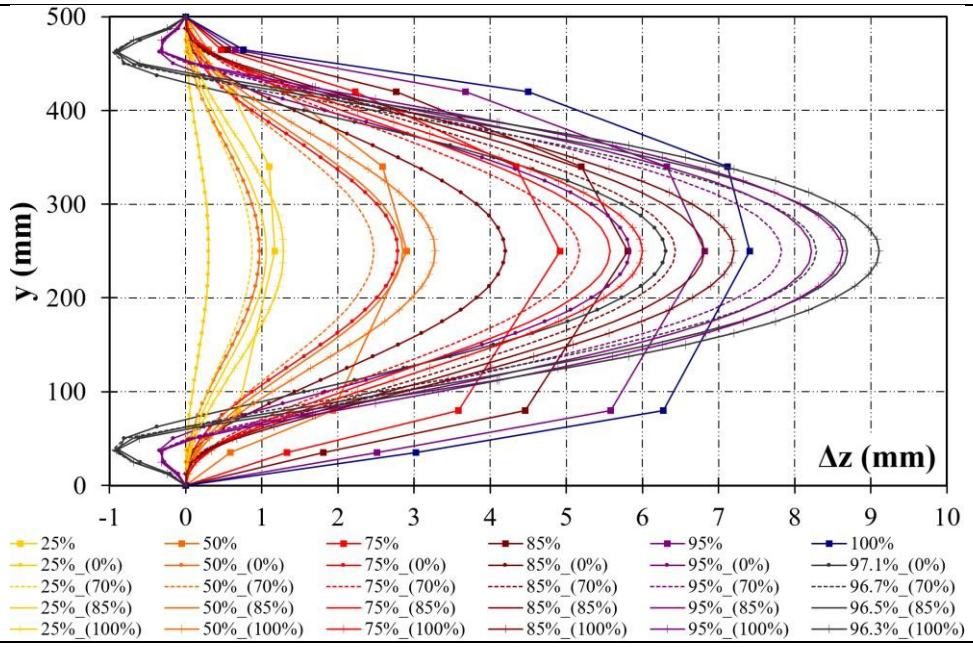


a) sample A1, middle section

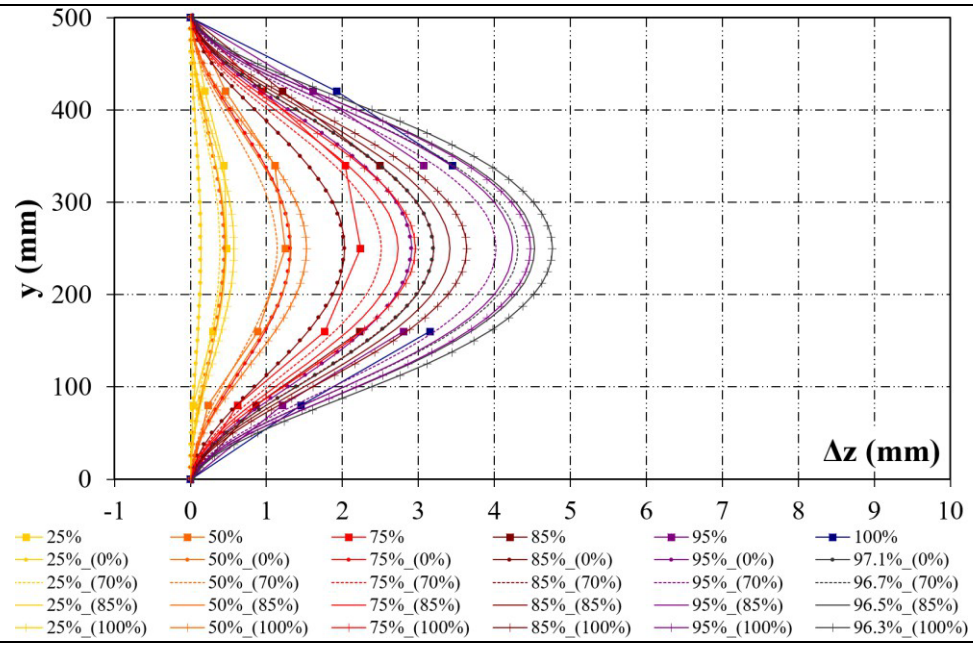


b) sample A1, edge section

Fig. 6: Out-of-plane displacements of the web girder in the sample A1

It can be seen that the maximum stresses reached in the panel are lower than the failure stress despite the plastic - hardening phase, this confirms that the crisis is reached by loss of stiffness as can be seen in Fig. 8a.

### *5.2. Sample 2A*

The process described before has been done even for sample 2A. As in the previous case, the ultimate experimental load is higher than the critical load from the numerical analysis. The post-critical resistance reserves of the panel increase the ultimate resistance by almost 30 % (see 6) while it reaches 19% when comparing to the full panel, leading to the conclusion of more plastic resources observed in this case. Moreover, both the shape and the magnitude of the initial imperfections do not show a clear influence on the ultimate resistance value.

| $F_{u,exp}$ | $F_{cr}$ | $F_{u,1°;5mm}$ | $F_{u,1°,2.5mm}$ | $F_{u,1°,1.25mm}$ | $F_{u,1°;0.75mm}$ | $F_{u,1°;0.5mm}$ | $F_{u,1°+2°;2.5mm}$ | $F_{u,1°+2°;1.25mm}$ |
|---|---|---|---|---|---|---|---|---|
| 307.8 | 218 | 267.7 | 268.6 | 269.1 | 269.3 | 270 | 268.3 | 269.1 |
| - | 70.8% | 87% | 87.3% | 87.4% | 87.5% | 87.7% | 87.2% | 87.4% |

Table 6: Critical and ultimate load from FEM analysis


| $F_{u,exp}$ | $F_{cr}$ | $F_{u,1°;5mm}$ | $F_{u,1°,2.5mm}$ | $F_{u,1°,1.25mm}$ | $F_{u,1°;0.75mm}$ | $F_{u,1°;0.5mm}$ | $F_{u,1°+2°;2.5mm}$ | $F_{u,1°+2°;1.25mm}$ |
|---|---|---|---|---|---|---|---|---|
| 307.8 | 218 | 267.7 | 268.6 | 269.1 | 269.3 | 270 | 268.3 | 269.1 |
| - | 70.8% | 87% | 87.3% | 87.4% | 87.5% | 87.7% | 87.2% | 87.4% |


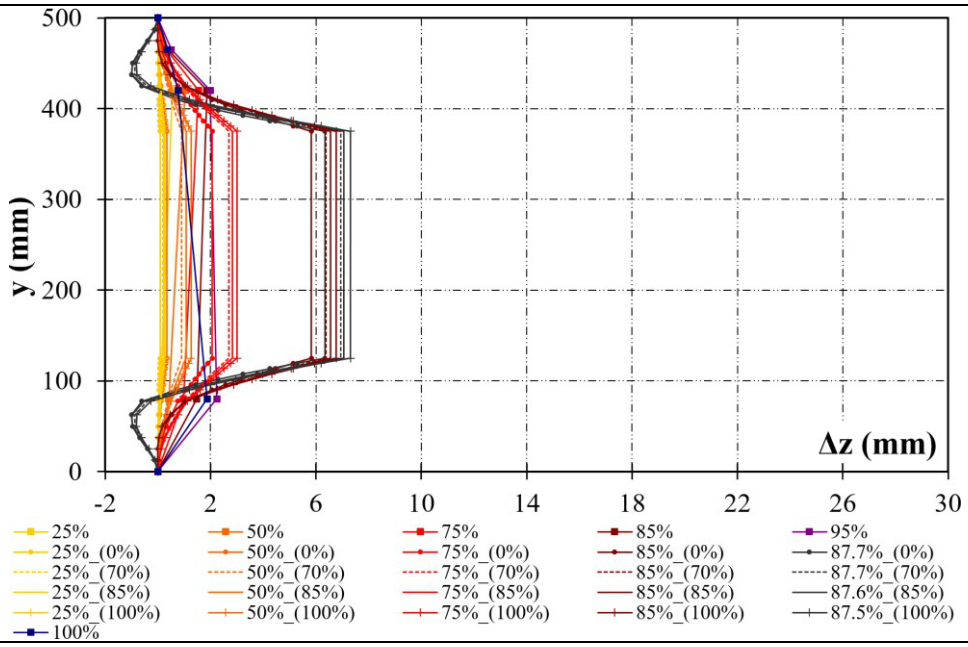

a) sample A1, middle section

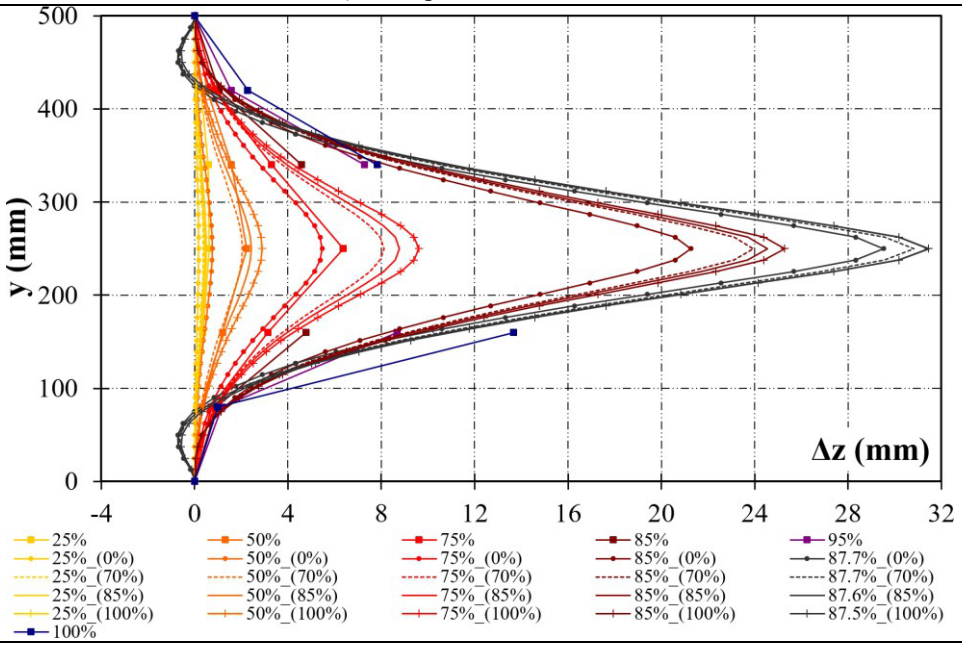


b) sample A1, edge section

Fig. 7: Out-of-plane displacements of the web girder in the sample 2A

From the FEM results, it should be noted that when approaching the ultimate load, the web panel undergo a large distortion at the sides of the opening, see Fig. 7. The differences in terms of displacement between the numerical analysis (curves obtained for different values of the peak residual stress) and the experimental curves are motivated by the fact that both refer to a certain percentage of the experimental ultimate load which, being in this case rather greater than the numerical one, implicitly leading to such differences. It has been seen that the evolution of the stress is quite uniform quantitatively and qualitatively and the maximum Von Mises stresses observed are around 500 MPa (Fig. 8b).

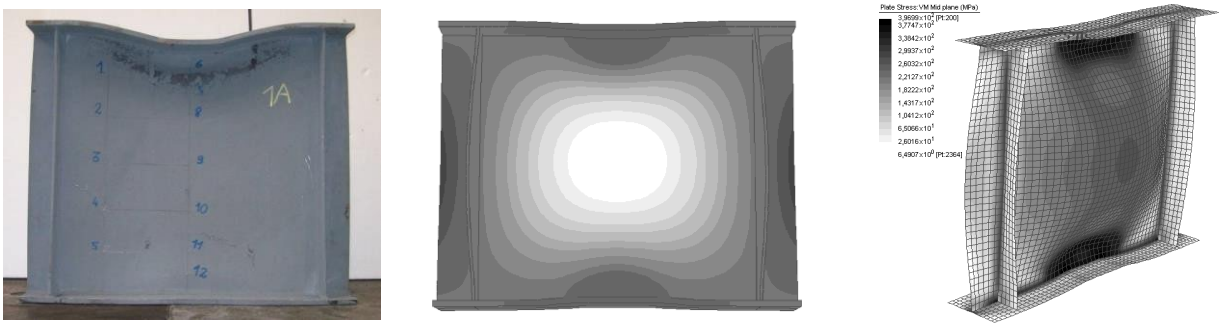

a) specimen 1A

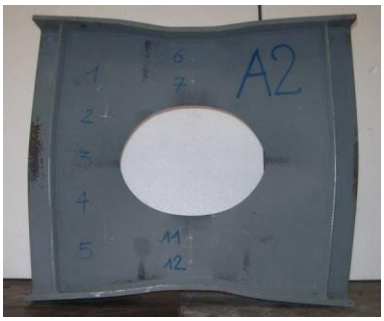


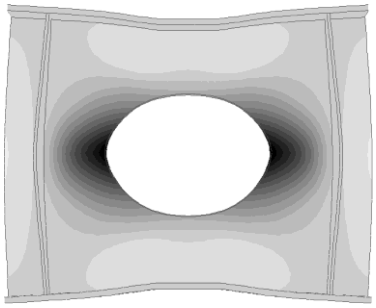

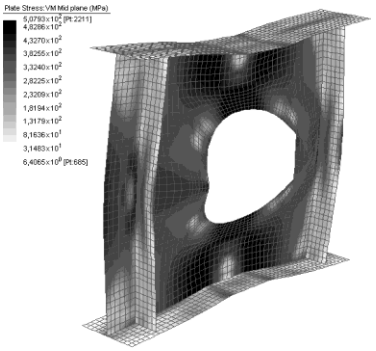


b) specimen 2A


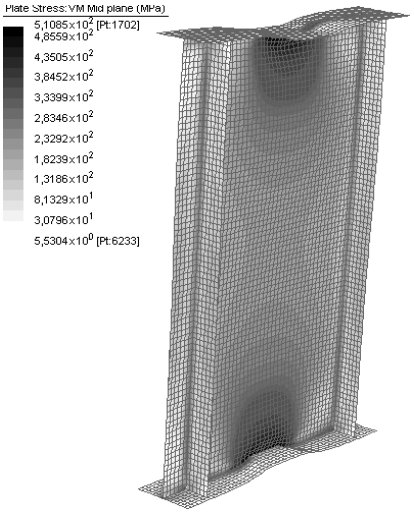


c) specimen 3A


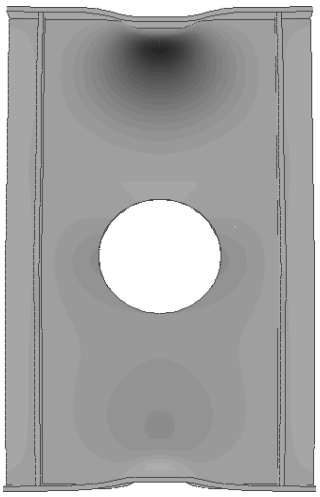

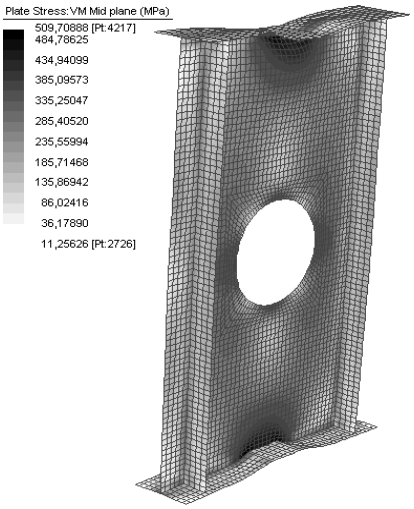


d) specimen 4A

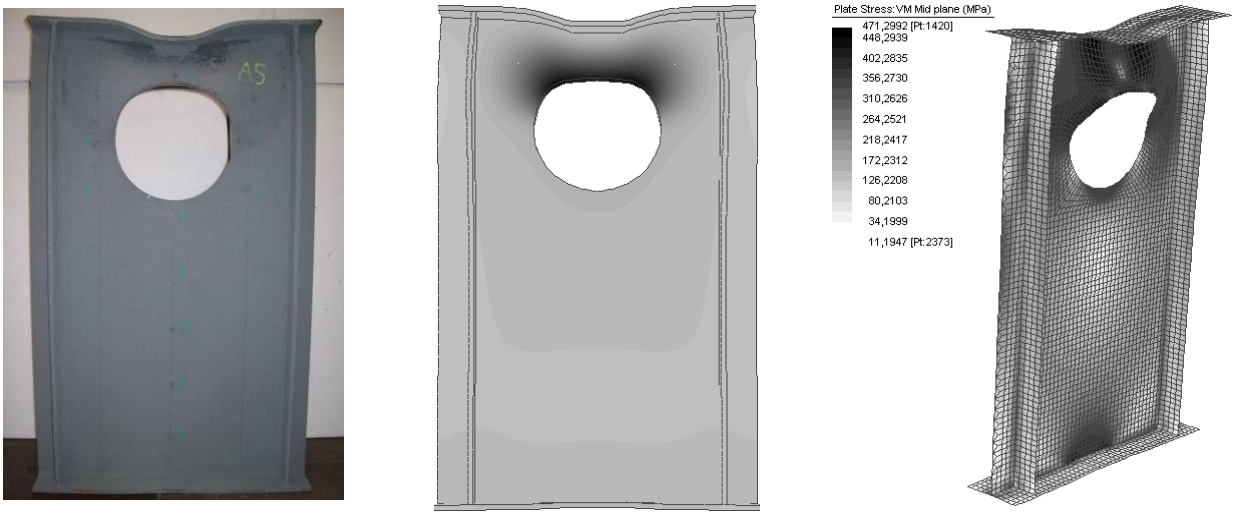


e) specimen 5A

Fig. 8: Experimental versus Numerical deformed shape of the specimens A

### *5.3. Sample 3A*

In this case, the critical load is almost three times higher than the experimental ultimate load despite the slenderness of the girder, see Table 7. The outcome can be justified by the short panel aspect ratio and the interaction between the vertical stiffeners and the flanges, which increase the stiffness of the whole girder. Besides, the non-linear analysis revealed that shape and amplitude of the imperfections have a significant influence on the ultimate strength of the panels. Finally, assuming initial imperfect girders in the numerical model, the best solutions reflecting qualitatively the out-of-plane displacement of the girders were obtained imposing the combination of the two first buckling modes as the imperfections shape.

Table 7: Critical and ultimate load from FEM analysis

| $F_{u,exp}$ | $F_{cr}$ | $F_{u,1°;2.5mm}$ | $F_{u,1°,1.25mm}$ | $F_{u,2°,2.5mm}$ | $F_{u,2°;1.25mm}$ | $F_{u,1°+2°;2.5mm}$ | $F_{u,1°+2°;1.5mm}$ | $F_{u,\ 1°+2°;1mm}$ |
|---|---|---|---|---|---|---|---|---|
| 911.9 | 2530 | 887.6 | 907 | 866.9 | 890.5 | 884.7 | 896.2 | 886.7 |
| - | 277% | 97.3% | 99.5% | 95.1% | 97.7% | 97% | 98.3% | 97.2% |

The effect of the residual stress on the web out-of-plane movements is quite relevant. Although, the qualitative form remains almost unchanged, the maximum Δz values are significantly increased by the presence of a residual stress field. In both graphs (see Fig. 9), it can be seen by including these stresses in the FEM that the numerical results are close to the real ones. This consideration is particularly evident for the last steps of the applied load where the experimental deformation is approached by the numerical curves in almost all the detection points. Finally, FEM models have confirmed that the panel collapses due to the loss of the steel's resistance reserves in concentrated zones before displaying the global instability as can be seen in the chromatic nuances (Fig. 8c).

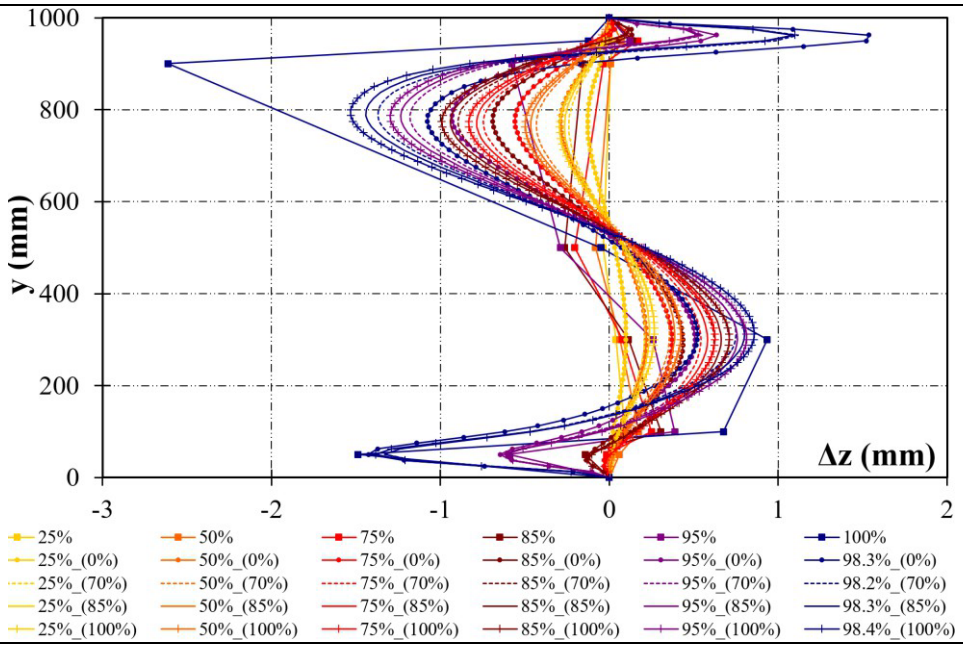


a) sample A1, middle section

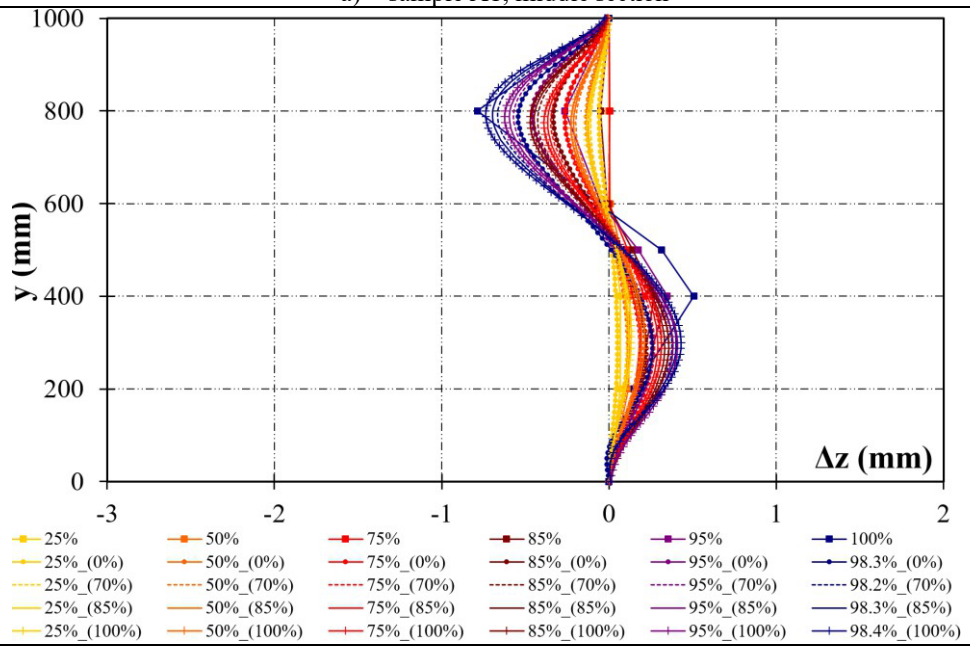


b) sample A1, edge section

Fig. 9: Out-of-plane displacements of the web girder in the sample 3A

### *5.4. Sample 4A*

The specimen is similar in geometry to the sample 3A but with the presence of a centred hole. Analogously to the previous case, the critical buckling load is more than three times higher than the experimental ultimate load.

The same observations are made when the influence of the imperfections geometry and its amplitude on the FEM ultimate resistance is studied (Table 8). On the other hand, compared to the previous model, the effect of residual stresses on the out-of-plane displacement is lower. The maximum displacement Δz are significantly increased only in the last load increments. It is probably due to the complex deformed shape

observed in this case: being more articulated, the various curves appear more superimposed in many areas in the initial phases (Fig. 10).

Table 8: Critical and ultimate load from FEM analysis

| $F_{u,exp}$ | $F_{cr}$ | $F_{u,1°;2.5mm}$ | $F_{u,2°,2.5mm}$ | $F_{u,1°+2°;5mm}$ | $F_{u,1°+2°;2.5mm}$ | $F_{u,3°;2.5mm}$ | $F_{u,5°;2mm}$ | $F_{u,\ 5°;1mm}$ |
|---|---|---|---|---|---|---|---|---|
| 883.5 | 2943 | 894.5 | 884.5 | 860.1 | 888.8 | 847.3 | 860 | 890.4 |
| - | 333 % | 101.2 % | 100.1 % | 97.4 % | 100.6 % | 95.9 % | 97.3 % | 100.8 % |

The peaks of the Von Mises stresses are concentrated in the two areas adjacent to the load or support footprint and are concentrated in four symmetrical zones around the hole: the two lateral zones subject to prevalent compression and the upper and lower zones subject to prevalent traction. The contour of the out-of-plane displacement Δz presents a series of scale. The most altered zone is the one below the load. Moreover, it should be noted that the hole appears practically non-deformed (Fig. 8d).

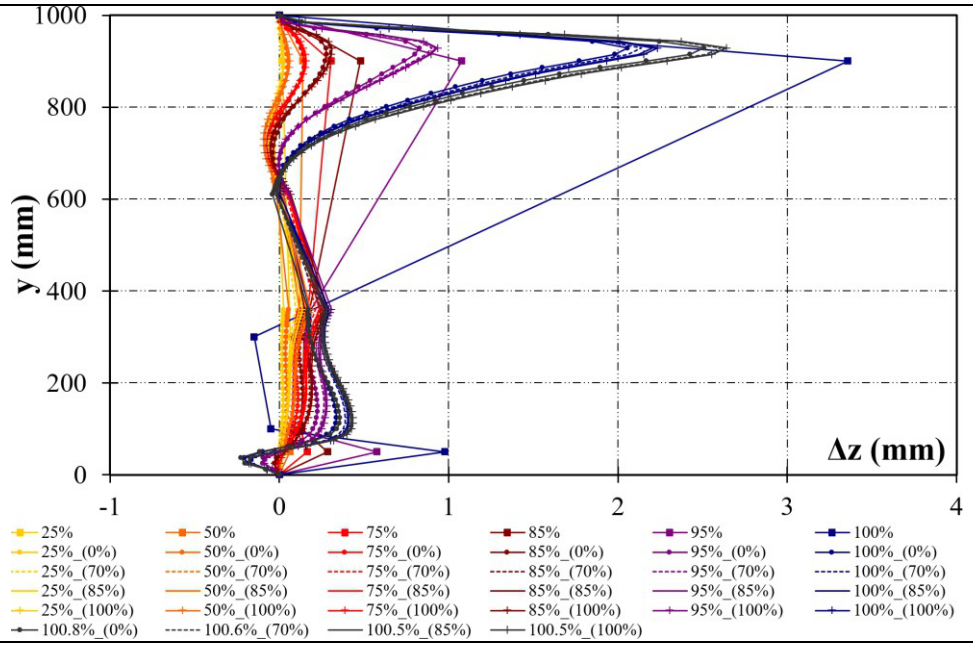

a) sample A1, middle section

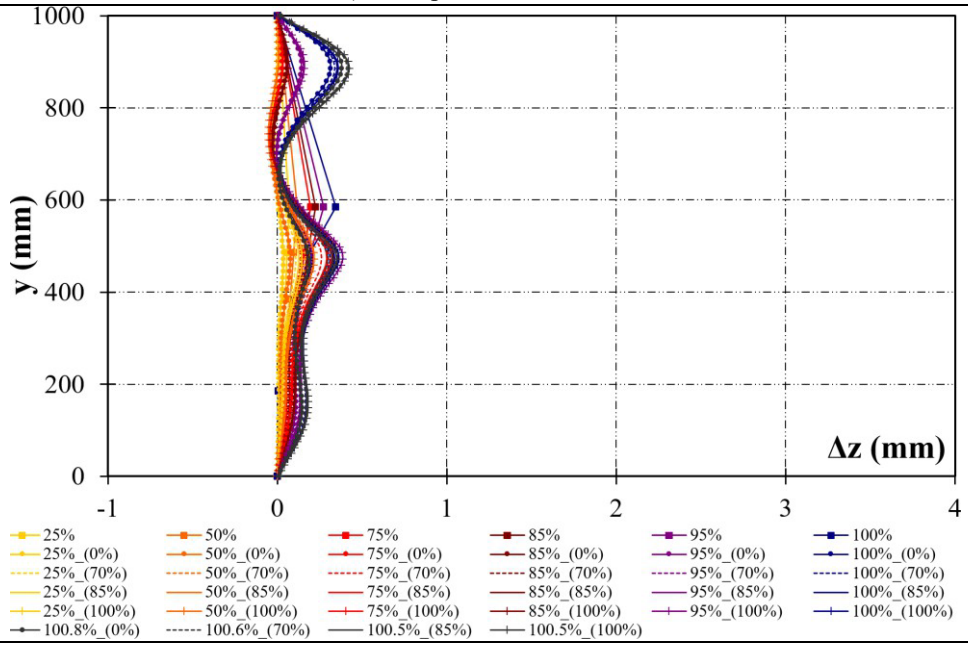


b) sample A1, edge section

Fig. 10: Out-of-plane displacements of the web girder in the sample 4A

### *5.5. Sample A5*

The last case of the slender girder specimen is a perforated girder with the hole closed to the upper flange. The buckling load is three times higher than the ultimate load found in the laboratory test.

The structure is weakened by the asymmetrical location of the hole. The same outcome was found in the parametric analysis conducted in [31]. A hole located at a point of flexure ($h_w/2$) of the critical deformation referred to the full web panel has no major consequences on the overall behavior, while if moved close to a maximum point ($h_w/4$ or $3h_w/4$), the reduction in resistance is significant (Table 9). Despite some small local differences, the numerical results approximate the experimental ones sufficiently well. In the first graph (Fig. 11a), some discordances are observed in the lower part of the panel especially in correspondence of $F_{u,exp}$ whereas in the second graph (Fig. 11b) shape and entity of the displacements appear consistent with those detected in each zone of the panel.

Table 9: Critical and ultimate load from FEM analysis

| $F_{u,exp}$ | $F_{cr}$ | $F_{u,1°;5mm}$ | $F_{u,1°,3.5mm}$ | $F_{u,1°;2mm}$ | $F_{u,3°;1.25mm}$ | $F_{u,5°;5mm}$ | $F_{u,5°;2mm}$ | $F_{u,\ 5°;1mm}$ |
|---|---|---|---|---|---|---|---|---|
| 695.9 | 2150 | 675.2 | 686.4 | 695.9 | 762.3 | 673.1 | 695.2 | 701.5 |
| - | 309 % | 97 % | 98.6 % | 100 % | 109.5 % | 96.7 % | 99.9 % | 100.8 % |

The maximum Von Mises stresses are found in the area between the hole and the localized load. These stresses confirm the entry of the panel in plastic phase, but they are still lower than the ultimate value ($F_u \approx$ 500 MPa). Unlike the two previous cases (Samples 4A and 3A), the stress in this case do not reach the maximum implemented value. It can be noticed that in every configuration considered their peak value is

slightly higher than 470 MPa. On the other hand, the section is locally deformed in the area weakened by the hole (Fig. 8e). The panel deforms locally in a noticeable manner, due to the significant tension concentrations localized in this area while the remaining areas undergo much less deformation. The structural failure can therefore be classified as a local elasto-plastic buckling caused by the reduction in stiffness due to the proximity of the opening to the loaded edge of the panel.

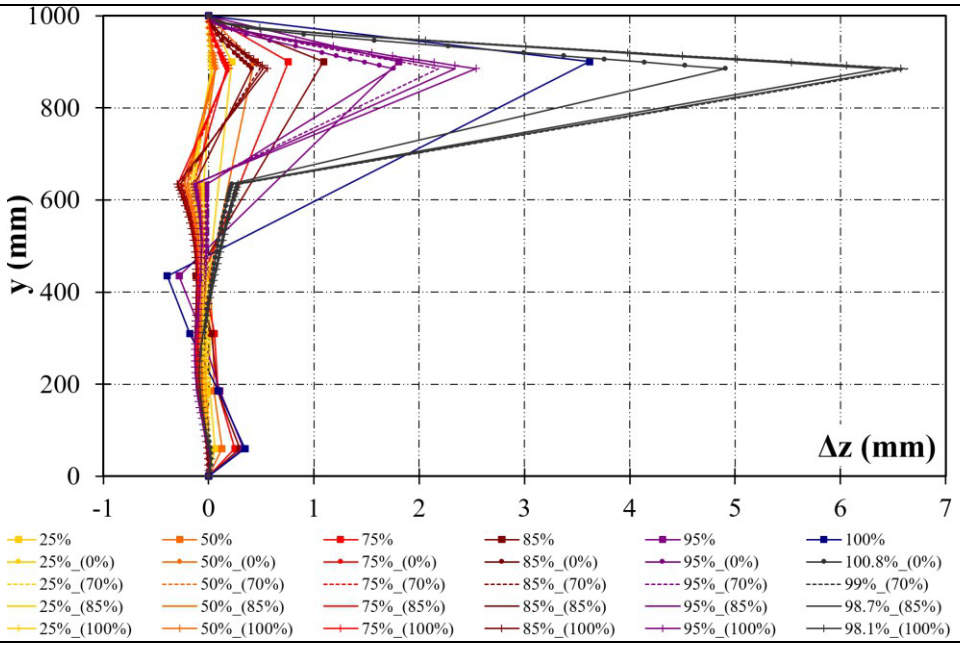


a) sample A1, middle section

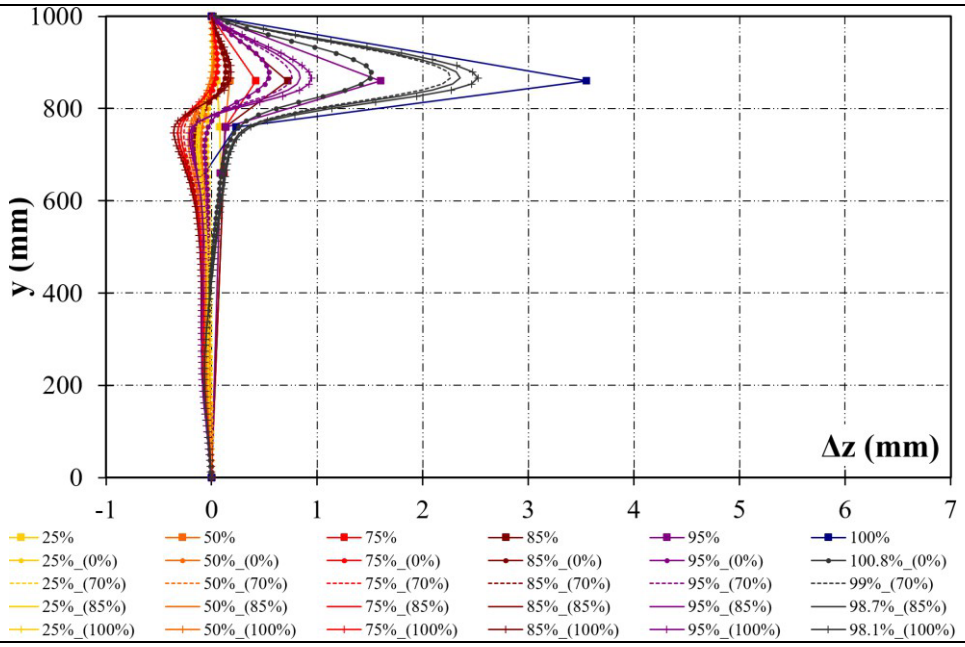


b) sample A1, edge section

Fig. 11: Out-of-plane displacements of the web girder in the sample 5A

### *5.6. Sample 1B*

Sample 1B differs to Sample 1A in the thickness of the web and the vertical stiffeners now being 10 mm. Unlike the results observed in Sample 1A, the critical buckling load in the case is 2.5 higher than the

ultimate experimental load since the girder under study is thick enough to fail under local instability (Table 10). The imperfections present at the beginning of the test are enhanced by the increase of applied loads and in such a case induce global and local deformations such as to speed up the plasticization of the section. The maximum displacements following these phases are in any case not negligible and are about 5.3 mm at the most deformed point (Fig. 12).

Table 10: Critical and ultimate load from FEM analysis

| $F_{u,exp}$ | $F_{cr}$ | $F_{u,1°;5mm}$ | $F_{u,1°,2.5mm}$ | $F_{u,1°,1.25mm}$ | $F_{u,1°+2°;5mm}$ | $F_{u,1°+2°;2.25mm}$ |
|---|---|---|---|---|---|---|
| 837.1 | 2096 | 820.7 | 847 | 870.1 | 826.4 | 844.1 |
| - | 250.4% | 98% | 101.2% | 103.9% | 98.7% | 100.8% |

It is possible to notice despite the overlaying of many curves, how the presence of residual stresses increases the deformation at the early stage of loads application. The general shape of the deformed remains as always the same. Compared to the previous cases, it seems that the effect of auto-stress is slightly lower for panel 1B. In particular, there are no great increases in Δz from the case of residual stresses equal to 70%$f_y$ to the maximum value of the same. Including this state of stress in the FEM, it is possible, however, to say that the numerical results are close to the experimental ones especially in the side section (Fig. 12a). In the middle section (Fig. 12b), the biggest differences are in the lower part of the panel due to the particular initial deformation. The solution obtained appears in any case adequate considering that the collapse load level reached is almost equal to that measured in the laboratory.

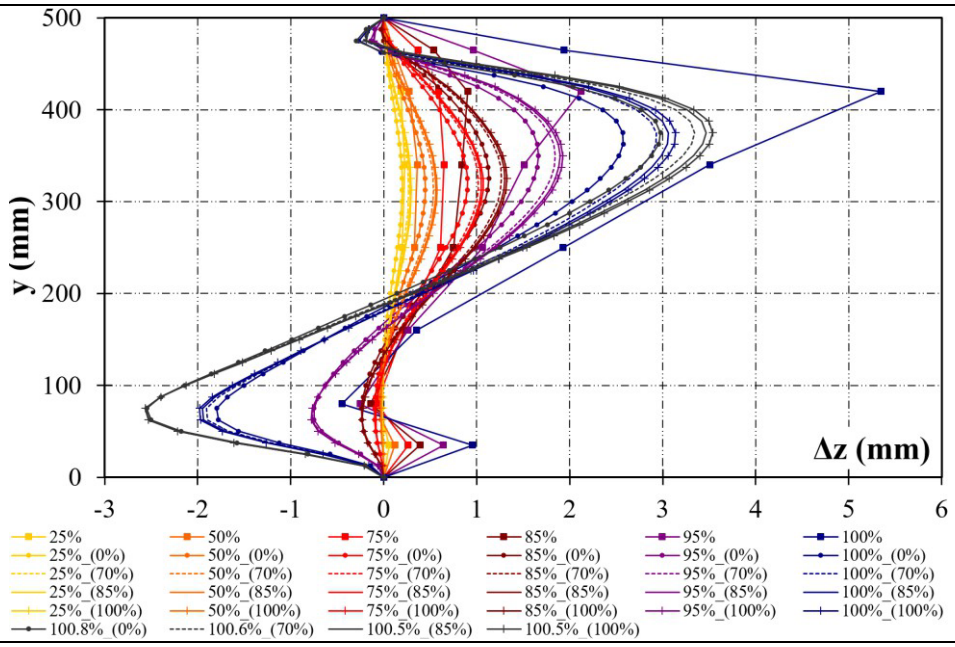

a) sample A1, middle section

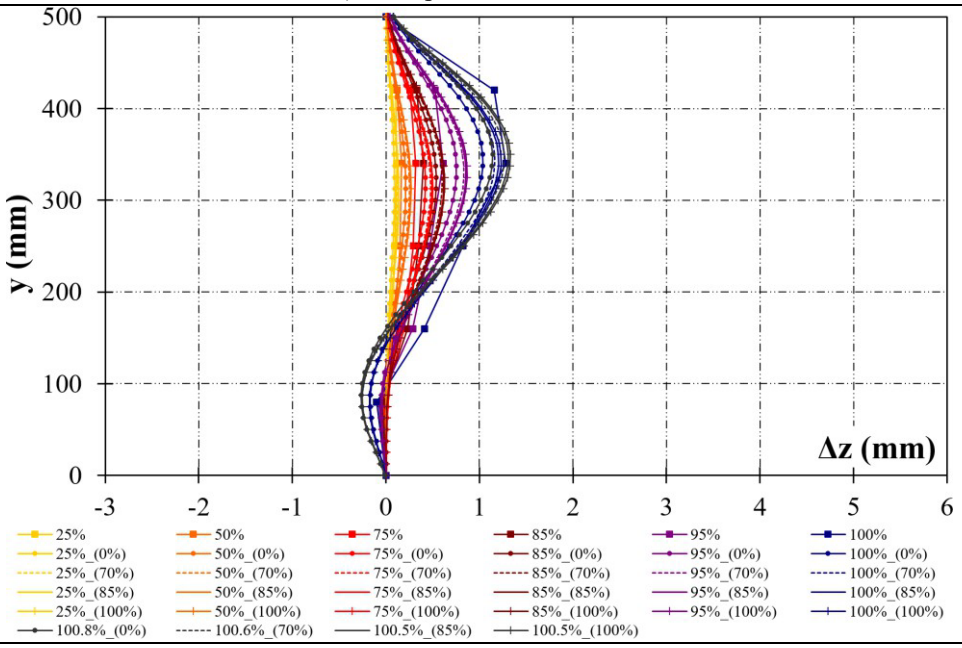


b) sample A1, edge section

Fig. 12: Out-of-plane displacements of the web girder in the sample 1B

The Von Mises stresses confirm that the material's resistance reserves has been fully used. The chromatic nuances adopted in the post-processing phase in the numerical study allow to better understand the shape assumed by the panel at the end of the load compared to the laboratory result (Fig. 17a).

*5.7. Sample 2B*

From an examination of modal forms in linear buckling analysis, first buckling mode shows a similar configuration to the experimental campaign in the side section while the third mode reflects the same test observation in the central region. Therefore, the combined two buckling modes will be considered for further analyses. The results in terms of the critical load is similar to the previous case (Sample 1B) with the buckling load being almost 2.7 times higher than the ultimate load (Table 11). The following diagrams (Fig. 13) illustrate the progression of out-of-plane displacements for some significant load levels.

The effect of the residual stress is evident. The shape assumed by the panel remains almost unchanged, but the extent of the displacements increases significantly. In both graphs, there are still strong differences between the numerical derivation curves and the experimental ones, confirming the difficulties to describe the phenomenon in the case of a thick panel. In particular, it can be noted that the first buckling mode prevails over the third as the load increases so that the panel tends to assume a symmetrical deformation with respect to the horizontal axis. Although numerical models provide higher collapse loads than the laboratory one, the deformed ones are greater than the experimental ones.

Table 11: Critical and ultimate load from FEM analysis

| $F_{u,exp}$ | $F_{cr}$ | $F_{u,1°;2,5mm}$ | $F_{u,1°,1,25mm}$ | $F_{u,3°;2,5mm}$ | $F_{u,3°;1,25mm}$ | $F_{u,1°+3°,2.5mm}$ | $F_{u,1°+3°,1.75mm}$ | $F_{u,1°+3°,1.25mm}$ |
|---|---|---|---|---|---|---|---|---|
| 591.4 | 1576 | 586.8 | 612.1 | 583.5 | 589.3 | 589 | 607.9 | 609.3 |
| - | 266.5 % | 99.2 % | 103.5 % | 98.7 % | 99.7 % | 99.6 % | 102.8 % | 103 % |

It is immediately noticeable how the stress field is uniform in qualitative and quantitative terms. The peak Von Mises stress reached their maximum value (about 500 MPa). The final configuration of the panel in both experimental and FEM campaign is very similar (Fig. 17b). The circular hole is changing into an oval shape and compared with the one in case 2A, the deformation of the perimeter of the hole is much smaller in this case.

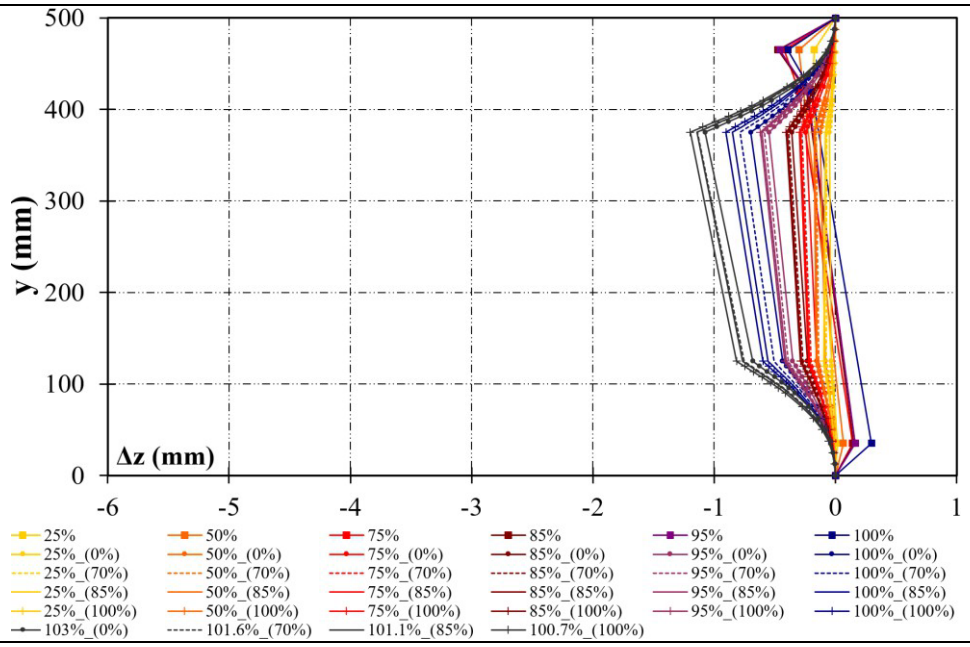


a) sample A1, middle section

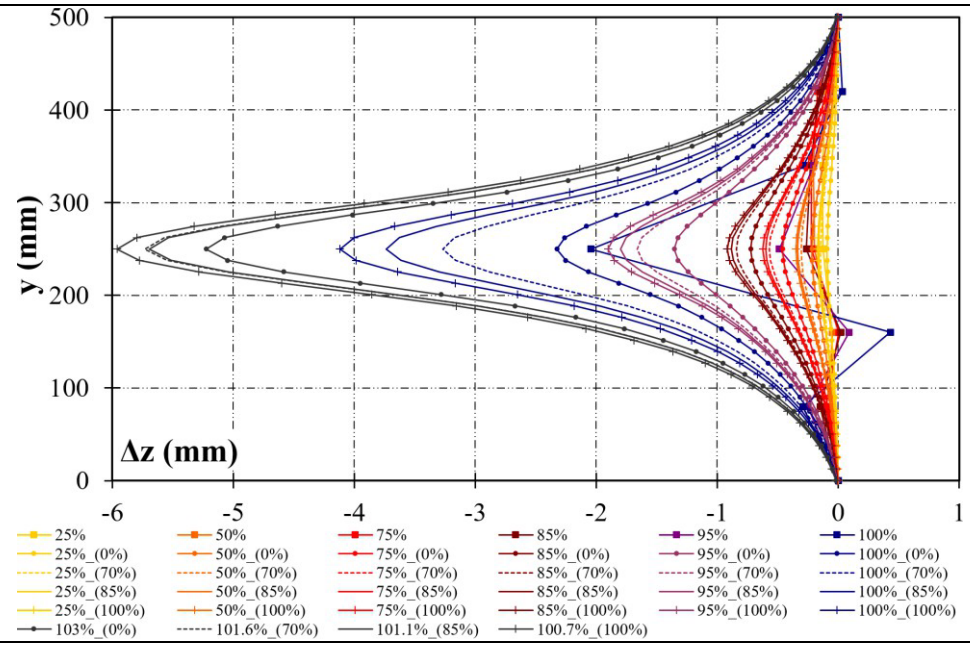


b) sample A1, edge section

Fig. 13: Out-of-plane displacements of the web girder in the sample 2B

*5.8. Sample 3B*

The comparison between experimental collapse load and linear critical load gives an extremely high result. The ratio were 2.5 and 2.66 respectively for Sample 1B and 2B. The panel in question is extremely stocky (Table 12) with the critical buckling reaching six times the experimental collapse load and the crisis is linked to the exhaustion of the resistance reserves of the section. The structural response in the presence of a residual stress field at the perimeter was evaluated and the initial deformation was assumed to give the best results, with maximum out-of-plane displacements (Δz) equal to 3 mm. From the diagrams relative to the out-of-plane displacements (Fig. 14), a strong diversity of the behaviour is evident. Indeed, it is observed from both graphs that there are still some differences between the numerical curves and the experimental ones as in Fig. 14b, confirming the difficulties to describe the phenomenon in the case of a thick panel. On the other hand, the extent of the experimental displacements is confirmed by the numerical model in both situations despite different general shapes and the maximum displacement Δz represents $t_w$/13 and $t_w$/35 respectively in the middle and side section.

Table 12: Critical and ultimate load from FEM analysis

| $F_{u,exp}$ | $F_{cr}$ | $F_{u,1mm}$ | $F_{u,2mm}$ | $F_{u,3mm}$ | $F_{u,5mm}$ |
|---|---|---|---|---|---|
| 3442.7 | 21225 | 3531 | 3502 | 3471 | 3434.6 |
| - | 616.5 % | 102.5 % | 101.7 % | 100.8 % | 99.8 % |

The concentrated compression stress flow in particular in the areas close to the localized loads is clearly visible. The stress field obtained is also influenced by the initial panel geometry. The considerable structural rigidity guarantees the overall stability of the structure until the plasticisation of these areas; once the plastic reserves and the possibility of redistribution of the stresses are exhausted, the panel collapses with mainly vertical deformations: with respect to the latter, the displacements outside the plane are negligible. The final configuration of the panel appears rather similar in both FEM and experimental test (Fig. 17c). In particular, the most visibly compromised areas are those close to the localized load and the lower support. The real case highlights the deformation asymmetry between the two flat flanges, while the numerical model clearly behaves in a uniform way.

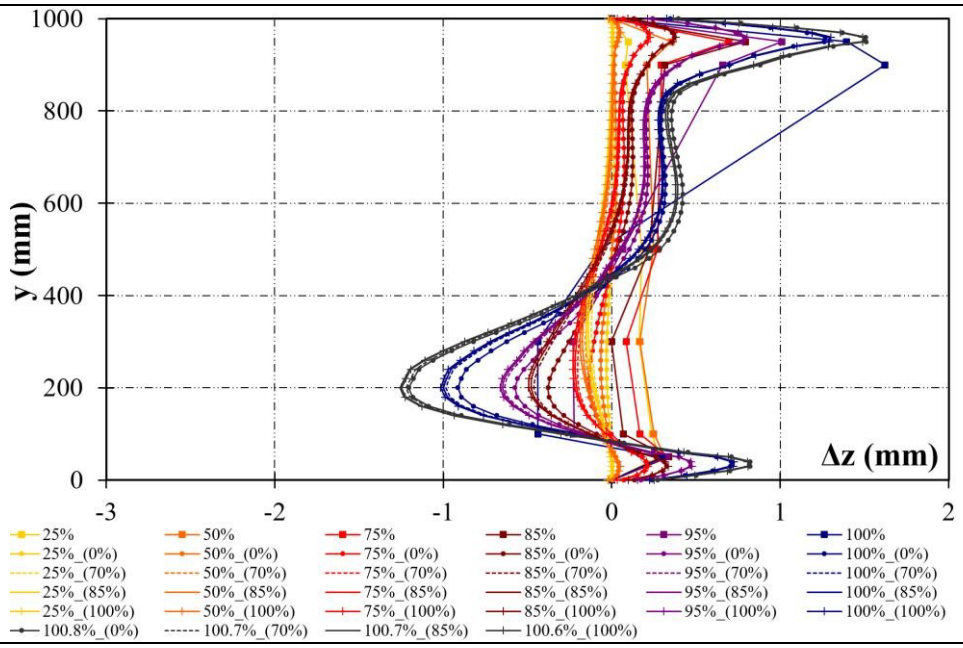


a) sample A1, middle section

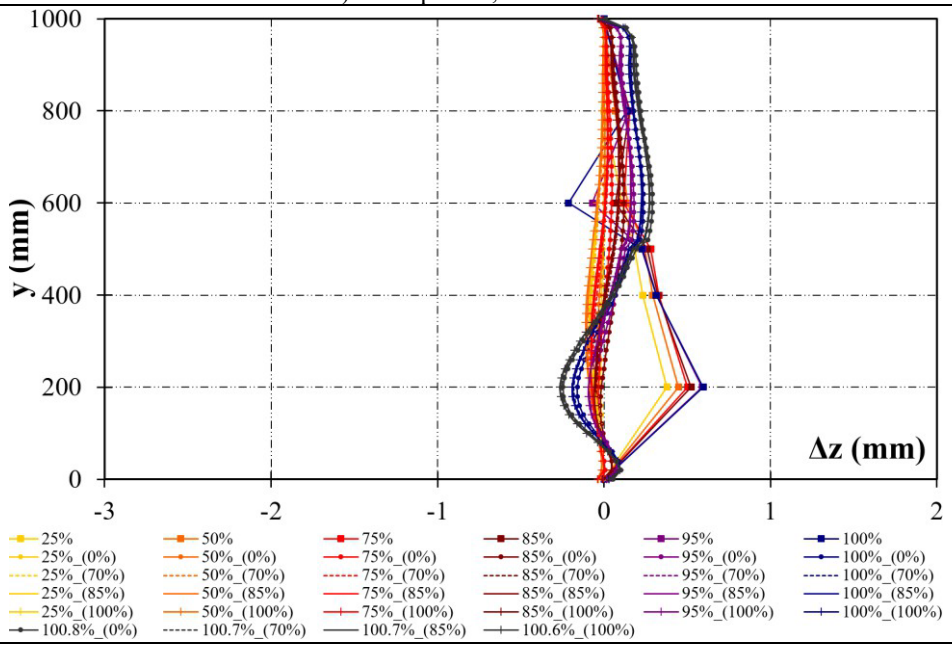


b) sample A1, edge section

Fig. 14: Out-of-plane displacements of the web girder in the sample 3B

### 5.9. Sample 4B

In this case, the critical load deduced from linear stability analysis is much higher than the ultimate experimental load (Table 13). In addition, the outcome of the non-linear analysis shows that the magnitude and general shape of the initial imperfections has little influence on the ultimate strength value; in any case, the collapse load remains close to 98% of the experimental value. As before (specimen 3B), the failure related to

the yielding of the material is hardly affected by the real structural geometry, which reduces the material's resistance resources, but to a much lesser extent than in slender structures.

The maximum experimental displacements detected in the two measurement sections are comparable with each other, but the resulting trend is rather uneven. The effect of the residual stresses is also in this circumstance rather modest. The numerical curves referred to the same load level are very close to each other; the out-of-plane displacements, however, are increased in the presence of this stress state, while the qualitative form remains the same. The numerical model despite different general shape roughly confirms the extent of the experimental displacements and the maximum displacement Δz is represented in the order of $t_w$/15 and $t_w$/13 respectively in the central and side section (Fig. 15).

Table 13: Critical and ultimate load from FEM analysis

| $F_{u,exp}$ | $F_{cr}$ | $F_{u,1°;1mm}$ | $F_{u,1°,5mm}$ | $F_{u,2°;1mm}$ | $F_{u,2°;2mm}$ | $F_{u,2°,4mm}$ | $F_{u,3°,1.75mm}$ | $F_{u,\ 3°,2mm}$ |
|---|---|---|---|---|---|---|---|---|
| 3578.0 | 24450 | 3506 | 3468.6 | 3520 | 3514 | 3503.6 | 3523 | 3516 |
| - | 683.3 % | 98.0 % | 96.9 % | 98.4 % | 98.2 % | 97.9 % | 98.5 % | 98.3 % |

This initial coaction state does not seem to change significantly the final distribution of efforts. The same observation was made for the precedent sample 1B, 2B and 3B. The effect of the residual stresses was, among other things, negligible with respect to the ultimate load and the structural stability is guaranteed by a high overall stiffness. In correspondence with the ultimate load, the out-of-plane displacements remain rather limited and certainly much lower than the in plane ones. From the FEM, it is shown that the web panel appears practically flat, while the most stressed zone is suffering a quite consistent vertical displacement. Finally, the deformation observed during the laboratory test is much more close to the final outcome of the FEM analysis (Fig. 17d).

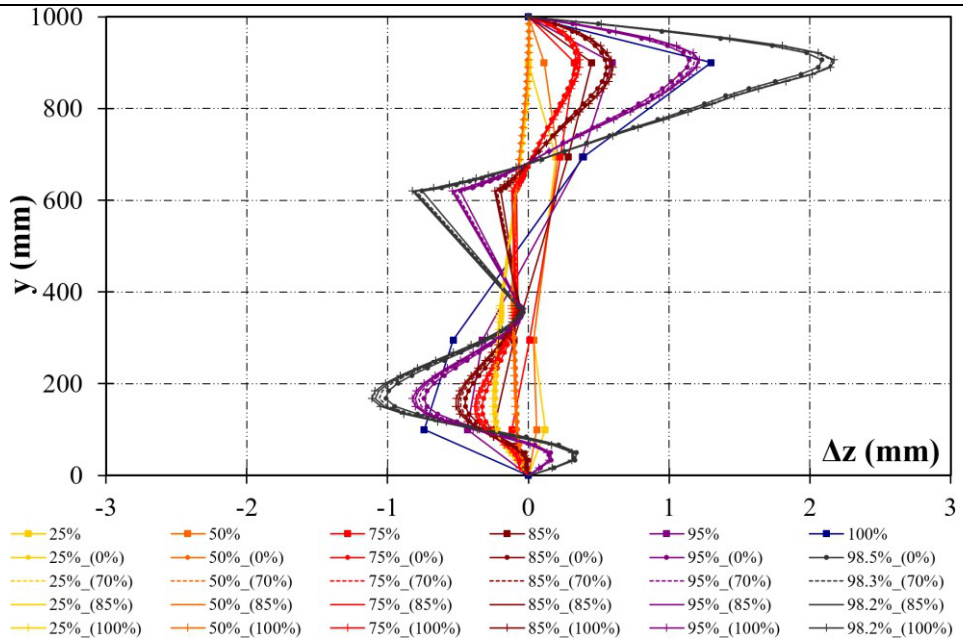

a) sample A1, middle section

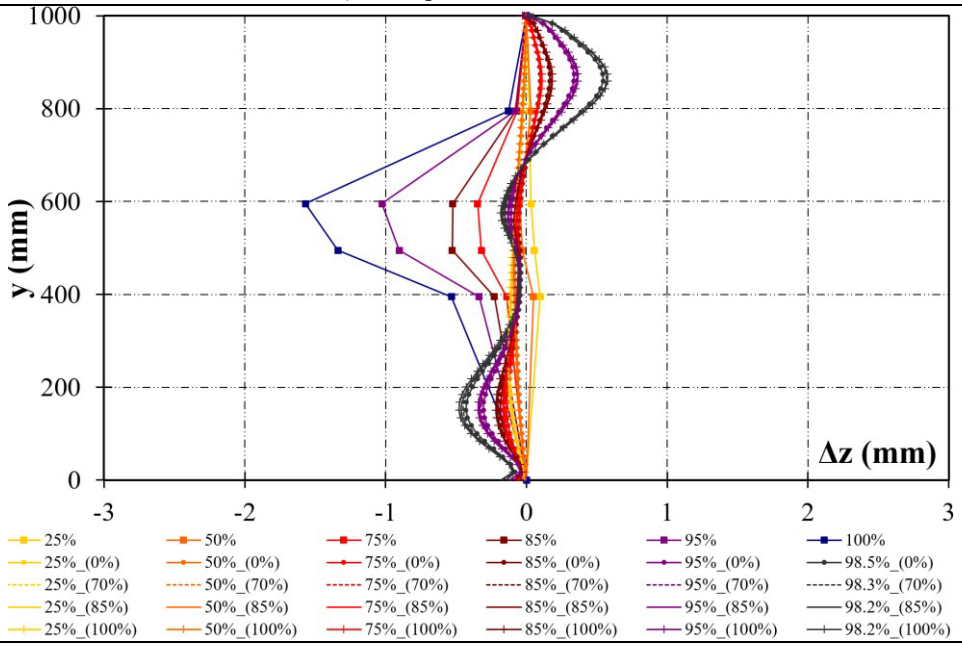


b) sample A1, edge section

Fig. 15: Out-of-plane displacements of the web girder in the sample 4B

## 5.10. Sample 5B

The last case of the Samples B shows the same trend than the previous case with the critical buckling load higher about six times the experimental ultimate load (Table 14). The maximum experimental displacements detected in the two measurement sections are clearly different from each other. To guarantee the same scale of the x-axis, the first diagram (Fig. 16a) appears much more flattened than the second (Fig. 16b).

From the two figures, it is clear that the numerical curves referring to the same load level are very close to each other. In particular, the most deformed areas is observed between the hole and the upper edge of the panel in a lateral position, while in the central part the web, distortions seem much more contained. The out-of-plane displacements are slightly increased due to the residual stresses, while the qualitative form remains the same. The modest effect of the residual stresses is confirmed in the two previous models (sample 3B and 4B).

Table 14: Critical and ultimate load from FEM analysis

| $F_{u,exp}$ | $F_{cr}$ | $F_{u,1°;1mm}$ | $F_{u,1°,2mm}$ | $F_{u,2°;1mm}$ | $F_{u,3°;1mm}$ | $F_{u,3°,2mm}$ |
|---|---|---|---|---|---|---|
| 3089.1 | 18130 | 2963.6 | 2941.2 | 2953.6 | 2981.1 | 2946.3 |
| - | 586.9 % | 95.9 % | 95.2 % | 95.6 % | 96.5 % | 95.4 % |

The shape assumed by the circular opening appears very deformed in the laboratory photo and the same aspect is reproduced in output by the numerical model (Fig. 17e). The lower flange is in both cases little deformed, while the upper one shows some considerable shape alterations due to the reduced structural rigidity due to the proximity of the opening.

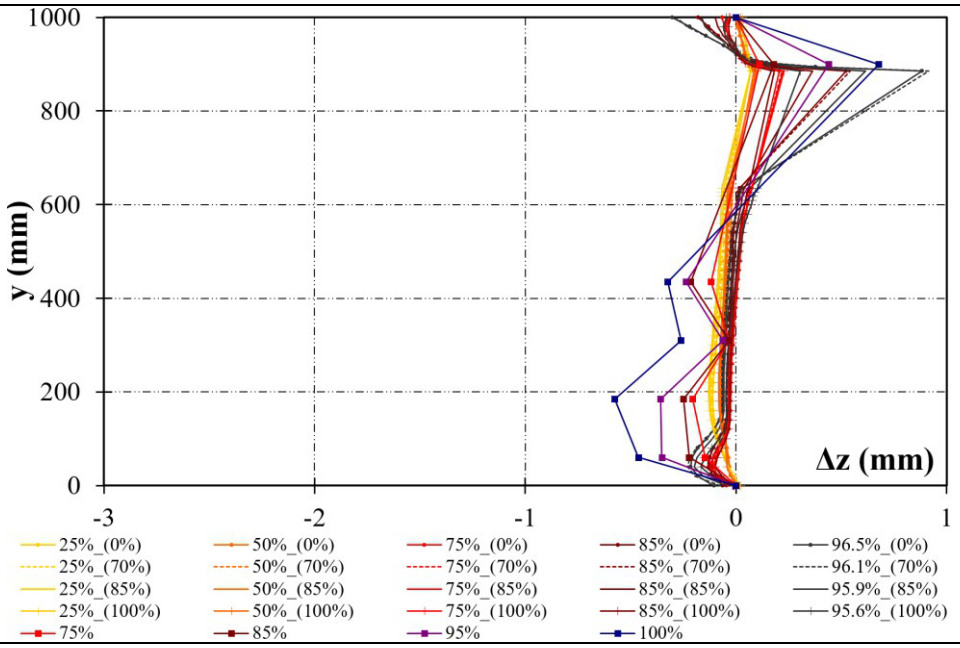


a) sample A1, middle section

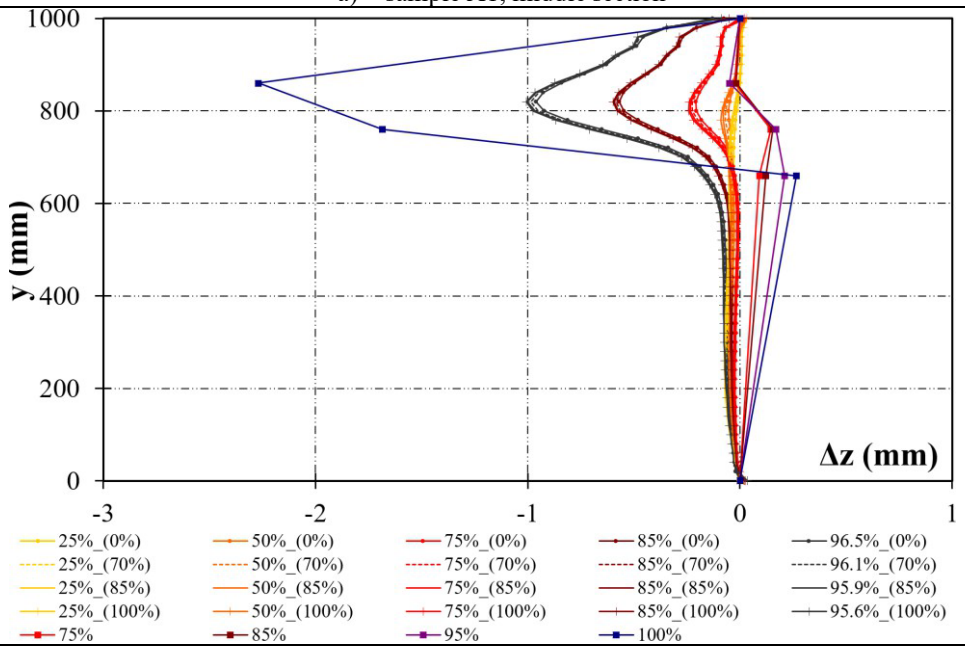


b) sample A1, edge section

Fig. 16: Out-of-plane displacements of the web girder in the sample 5B

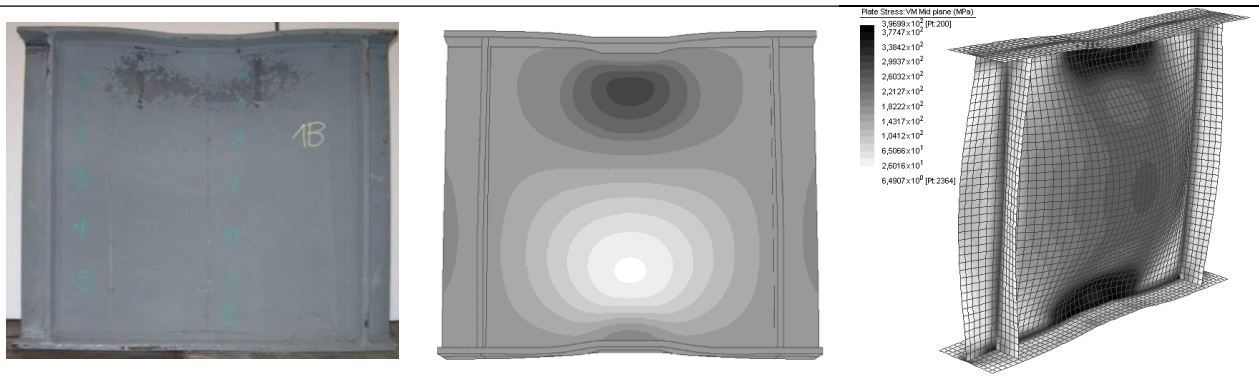


a) specimen 1B

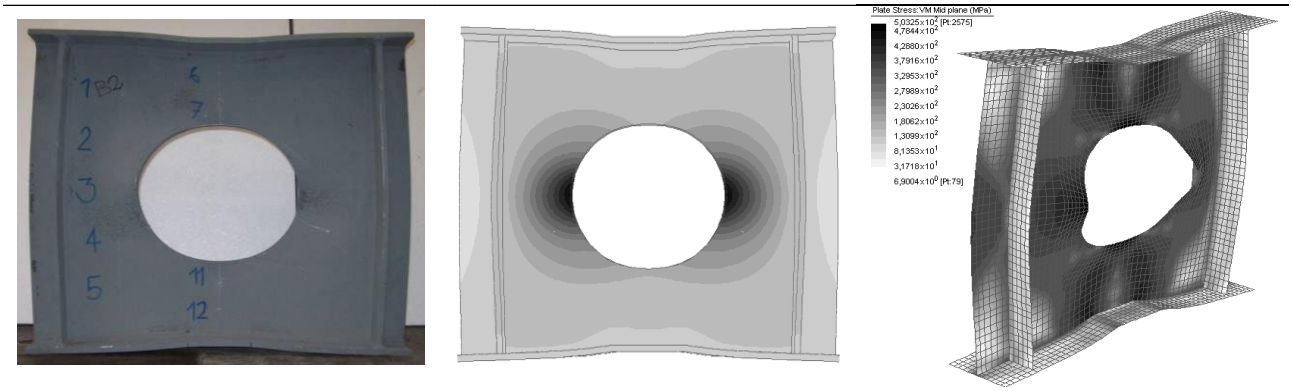


b) specimen 2B

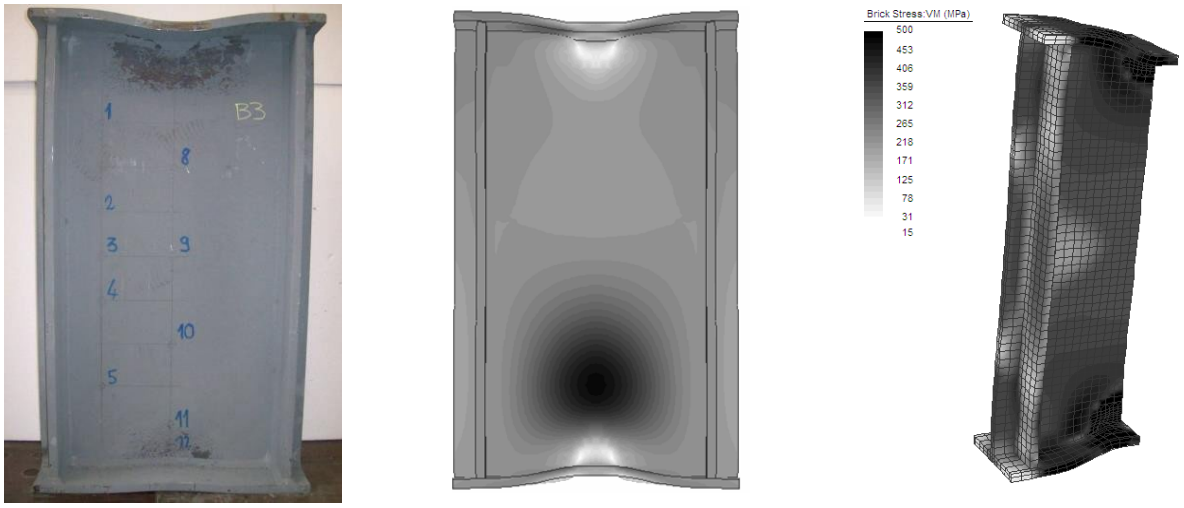


c) specimen 3B

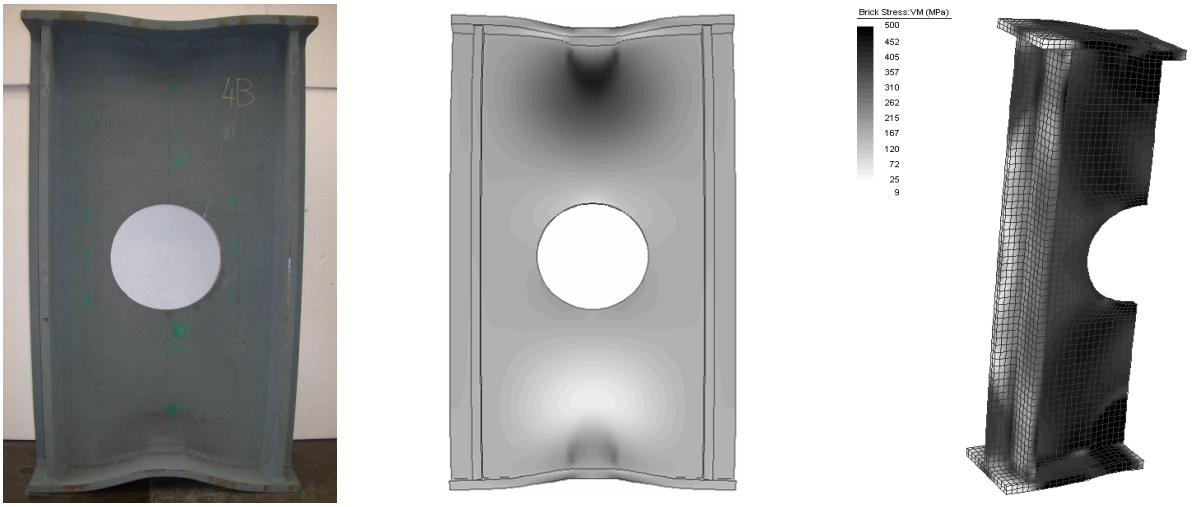


d) specimen 4B


e) specimen 5B

Fig. 17: Experimental versus Numerical deformed shape of the specimen B

### *5.11. Summary of the results*

Tables 5 to 14 summarise the overall results of the experimental campaign and the numerical analysis for critical buckling loads, ultimate load and the influence of imperfections. Although the numerical model was able to reproduce the actual behaviour of the panels sufficiently well, it was not possible to define a general trend that could conform to a wide range of cases.

In the second category of specimens, for instance samples B3, B4 and B5, it has been found that structural failure is associated with plasticization of the material and, even at higher load levels, orthogonal deformations at right angles to the plane are rather limited. In addition, sample 1B behaves qualitatively similar to samples 3A, 4A and 5A. The failure is associated with the plasticization of the material and not with the loss of equilibrium in the elastic field.

Finally, the analyses revealed that only panels 1A and 2A can be considered actually slender. The failure was mainly due to the loss of stability with subsequent local hardening of the material. The critical load of these two structures is lower than the experimental one due to the post-critical reserves. The underestimations provided are about 19% and 29% respectively. For these two cases, the assumption of the deformation corresponding to the first buckling mode appears to be the most correct choice to reproduce both the ultimate load and the progressive deformation of the panel.

### *5.12. Influence of residual stress on Von Mises analysis*

Finally, additional investigations on the influence of the applied load on the stress state were done on specimens 1A and 2A. The ideal Von Mises stress below the most stressed areas were considered and graded

according to the entity of the external force. The two graphs below give the results based on the variation of the residual stresses magnitude Fig. 18.

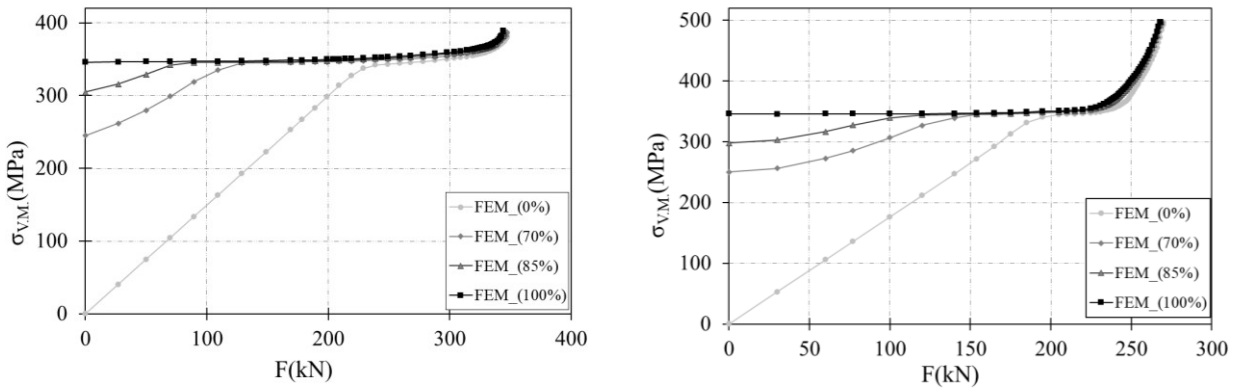


a) sample 1A b) sample 2A

Fig. 18: Von Mises stress versus applied force

Many conclusions can derived from the two figures. From the two diagrams, the effect of the residual stress is clear. Particularly, it is interesting to note that the presence of an initial compressive state reduces the elastic field until it is eliminated for the last case treated (FEM_(100%)). Once the yield strength limit has been reached at the most stressed point, the redistribution of the stresses allows the external load to increase. It can be seen that the end parts of the curves overlap almost perfectly. From these graphs it is then clear that in terms of ultimate strength the effect of welding residual stresses is practically null. Another observation should be made with regard to the load level at which the first yield strength occurs. The first trend reported in the two cases, FEM_(100%) and FEM_(85%), shows that this load value corresponds roughly to 68 to 72% of the final load, which is confirmed in [44], while in [43] the yield strength of the web panel starts at load values between 49% and 78% of the final value with an increasing percentage as the panel's slenderness increases. Considering that the two cases treated are rather slender plates, the results obtained can be considered largely satisfactory.

## 6. Conclusion

An extensive experimental analysis and FEM have been done in this study to characterize the behaviour of perforated steel girders under compression loads. Experimental campaigns have shown their importance to define an accurate numerical modelling that integrates the imperfections. Also, numerical analyses have confirmed the fact that a slender panel tends to follow the modal shape corresponding to the lower critical load, while for the small or intermediate ones it seems necessary to know the actual starting geometry in order to follow step by step the deformed profile under load as found in [26] and [31]. In particular, the following conclusions were drawn.

- The experimental tests reported in this document show that the analytical formulation proposed in the Eurocode is excessively conservative, providing a value of buckling strength below the experimental value of at least 40%, and beyond, both when the failure occurs in the elastic and plastic field. This

result highlights the importance of the experimental testing campaign developed and may be the starting point for the development of a new analytical formulation that produces results more in line with the experimental evidence than the current Eurocode formulation.

- The sample 1B showed a similar qualitatively behaviour to the specimen 3A, 4A and 5A. The failure is linked to the plasticization of the material even though the maximum final displacements are not negligible. Furthermore, the initial geometric imperfections obtained with the first buckling mode is not the most appropriate solution and the panel is clearly affected by the actual initial geometry. The residual stresses cause clear consequences with respect to the out-of-plane displacement $\Delta z$ even if to a seemingly lower extent compared to the previous cases. As for the three rectangular panels of case A, also in this circumstance the critical load is clearly higher than the last experimental one, confirming that the failure occurred is not related to the loss of equilibrium in the elastic field.

- The deformed configuration at failure of intact square panels shows a maximum out-of-plane displacement in the centre zone ("loss of overall stability") for the slender panel, while the stocky panel fails with a displacement developed mainly in the region immediately below the localised symmetrical load ("loss of local stability").

- The hole (both centred and eccentric) does not significantly change the deformation of the slender and stocky rectangular panels and generally causes more substantial out-of-plane displacements in the perforated rectangular panels. The centred hole (at the nodal point of the critical deformation) does not substantially modify the ultimate load, while the eccentric hole (at the maximum point of the deformation) leads to a reduction in the ultimate load of the rectangular panels.

- From the sensitivity assessment, the analysis revealed that the ultimate load predicted by the numerical model is quite in agreement with the experimental one when the real imperfections are kept below the standard limits (hw/100 or 5 mm). As far as the self-tensioning effect is concerned, it was found that at the ultimate load level their effect is almost always negligible, while at the deformation level they make the panel less rigid.

**References**


1. Kovesdi B, Alcaine J, Dunai L, Mirambell E, Braun B, Kuhlmann U. Interaction behaviour of steel I-girders Part I: Longitudinally unstiffened girders. Journ. of Const. Steel Res. 2014:103:344-353.
2. Loaiza N, Graciano C, Casanova E. Design recommendations for patch loading resistance of longitudinally stiffened I-girders. Eng Struct. 2018:171:747-758. https://doi.org/10.1016/j.engstruct.2018.06.019
3. Jager B, Kovesdi B, Dunai L. I-girders with unstiffened slender webs subjected by bending and shear interaction. Jour. of Constr. Steel Res. 2017:131:176-188.

4. Sinur F, Beg D. Moment–shear interaction of stiffened plate girders—Tests and numerical model verification. Jour. of Constr. Steel Res. 2013:85:116-129.
5. Amani, Alinia M, Fadakar M. Imperfection sensitivity of slender/stocky metal plates. Thin-Walled Struct. 2013:73:207-215.
6. Maiorana E, Tetougueni CD, Zampieri P, Pellegrino C. Interaction between patch loading, bending moment, and shear stress in steel girders. Journal of Zhejiang Univ-Sci A (Appl & Eng). 2019:20(6):389-410.
7. Hasan QA, Wan Badaruzzaman WH, Al-Zand AW, Mutalib AA. The state of the art of steel and steel concrete composite straight plate girder bridges. Thin-Walled Struct. 2017:119:988-1020. http://dx.doi.org/10.1016/j.tws.2015.01.014.
8. Tetougueni C, Maiorana E, Zampieri P, Pellegrino C. Plate girders behaviour under in-plane loading: A review. Eng Fail Anal. 2019:95:332-358.

   https://doi.org/10.1016/j.engfailanal.2018.09.021.
9. El-Sawy, Nazmi A. Effect of aspect ratio on the elastic buckling of uniaxial loaded plates with eccentric holes. Thin-Walled Struct. 2001:39:983-998.
10. Pellegrino C, Maiorana E, Modena C. Linear and non-linear behaviour of steel plates with circular and rectangular holes under shear loading. Thin-Walled Struct. 2009:47:607-616. https://doi.org/10.1016/j.tws.2008.11.001.
11. Maiorana E, Pellegrino C, Modena C. Elastic stability of plates with circular and rectangular holes subjected to axial compression and bending moment. Thin-Walled Struct. 2009:47:241-255. https://doi.org/10.1016/j.tws.2008.08.003.
12. Maiorana E, Pellegrino C, Modena C. Non-linear analysis of perforated steel plates subjected to localised symmetrical load. Journal Const. Steel Res. 2009:65:959-964. https://doi.org/10.1016/j.jcsr.2008.03.018.
13. Maiorana E, Pellegrino C, Modena C. Elasto-plastic behaviour of perforated steel plates subjected to compression and bending. Steel and Composite Struct. 2011:11(2):131-147.
14. Chen B, Wang J, Li C. Compression tests and numerical analysis of perforated plates containing slotted holes in steel pylons. Thin-Walled Struct. 2013:67:129-143. http://dx.doi.org/10.1016/j.tws.2013.02.005.
15. Özbek E, Aykaç B, Aykaç S. The effects of brick walls strengthened with perforated steel plates on frame behavior. Eng. Struct. 2017:189:62-76.
16. Saraçoğlu MH, Albayrak U. Linear static analysis of perforated plates with round and staggered holes under their self-weights. Res. Eng. Struct. Mat. 2016:2:39-47.

17. Saroha U. Analyse the Stress Concentration Effect of a Perforated Plate under Uniaxial Loading Using Ansys. Int. J of All Res. Edu. and Scient. Meth. 2017:5(2):39-47.
18. Competing G+D, Strand7 user's manual, 2005.
19. Kalita K, Halder S. Static Analysis of Transversely Loaded Isotropic and Orthotropic Plates with Central Cutout. J. Inst. Eng. India Ser. C. 2014:95:347–358. https://doi.org/10.1007/s40032-014- 0138-9.
20. Paik k. Ultimate strength of perforated steel plates under edge shear loading. Thin-Walled Struct. 2007:45:301-306.
21. Singh GT, Singh KD. Experimental investigation on performance of perforated cold–formed steel tubular stub columns. Thin-Walled Struct. 2018:131:107-121. https://doi.org/10.1016/j.tws.2018.06.042
22. Yu NT, Kim B, Li LY,Yuan WB. Distortional buckling of perforated cold-formed steel beams subject to uniformly distributed transverse loads. Thin-Walled Struct. 2020:1481:106-114. https://doi.org/10.1016/j.tws.2019.106569
23. Bahrebar M, Kabir MZ, Ziralian T, Hajsadeghi M, Lim BP. Structural performance assessment of trapezoidally-corrugated and centrally-perforated steel plate shear walls. Journ. Of Const. Steel Res. 2016:122:584-594. http://dx.doi.org/10.1016/j.jcsr.2016.03.030
24. Feng R, Zhan H, Meng S, Zhu J. Experiments on H-shaped high-strength steel beams with perforated web. Eng. Struct. 2018:177:374-394. https://doi.org/10.1016/j.engstruct.2018.08.059
25. Lian VT, Shanmugam NE. Openings in horizontally curved plate girder webs, Thin- Walled Structures. 2003:41:245–69.
26. Yang Z, Kim C, Cho C, Beom HG. The concentration of stress and strain in finite thickness elastic plates containing a circular hole. Intern. Journal of Solids and Struct. 2008:45:713-31.
27. Brown CJ, Yettram AL, Burnett M. Stability of plates with rectangular holes. Journal of Struct. Eng. 1987:113(5)1111–6.
28. Narayanan R, Al-Amery RI, Roberts TM. Shear strength of composite plate girders with rectangular web cut-outs. Journal of Const. Steel Res. 1989:12:151–66.
29. Roberts TM, Azizian ZG. Strength of perforated plates subjected to in-plane loading. Thin-Walled Struct. 1984:2(2):153–64.
30. Brown CJ, Yettram AL. The elastic stability of square perforated plates under combination of bending, shear and direct load. Thin-Walled Struct. 1986: 4(3):239–46.
31. Komur MA, Sonmez M. Elastic buckling behaviour of rectangular plates with holes subjected to partial edge loading. Journal of Const. Steel Res. 2015:112:54-60.

32. El-Sawy A, Nazmi, Martini M. Elasto-plastic buckling of perforated plates under uniaxial compression. Thin-Walled Struct. 2004:42:1083-1101.
33. Shakerley T, Brown C. Elastic buckling of plates with eccentrically positioned rectangular perforations. Intern. Journal of Mech. Sci.1996:38(9):825-838.
34. Shanmugam N, Thevendran V. Design formula for axially compressed perforated plates. Thin-Walled Struct. 1999:34:1-20.
35. Gheitasi A, Alinia MM. Slenderness classification of unstiffened metal plates under shear loading. Thin-walled Struct. 2010:48:508-518. https://doi.org/10.1016/j.tws.2010.02.004.
36. CNR 10011. Costruzioni di acciaio. Istruzioni per il calcolo, l'esecuzione, il collaudo e la manutenzione. 1988:86.
37. CNR 10030. Anime irrigidite di travi a parete piena. 1993:163:36.
38. European Standard EN 1993-1-5. Design of steel structures: Plated structural elements. 2006
39. Tsavdaridis KD, D'Mello C. Web buckling study of the behaviour and strength of perforated steel beams with different novel web opening shapes. Journal of Const. Steel Res. 2011:67:1605- 1620. https://doi.org/10.1016/j.jcsr.2011.04.004.
40. European Standard EN 10025-2. Hot rolled products of structural steels - Part 2: Technical delivery conditions for non-alloy. 2006.
41. European Standard EN 1993-1-1:2002. Design of steel structures: General rules and rules for buildings. 1994:3(1):96.
42. Pavlovčič L, Detzel A, Kuhlmann U, Beg D. Shear resistance of longitudinally stiffened panels- Part 1: Tests and numerical analysis of imperfections. Journal of Constr. Steel Res. 2007:63:337- 350.
43. Maiorana E, Pellegrino C, Modena C. Imperfections in steel girder webs with and without perforations under patch loading. Journal of Constr. Steel Res. 2007:63:337-350.
44. Amani M, Alinia MM, Fadakar M. Imperfection sensitivity of slender/stocky metal plates. Thin-walled struct. 2013:73:207-215. https://doi.org/10.1016/j.tws.2013.08.010.